# THE VIKING ATMOSPHERE STRUCTURE EXPERIMENT – TECHNIQUES, INSTRUMENTS, AND EXPECTED ACCURACIES

ALVIN SEIFF
*Ames Research Center, NASA, Moffett Field, California*

(Received 10 October 1975)

**Abstract.** During high speed entry and descent through the atmosphere of Mars, the two Viking spacecraft will make in situ measurements of the structure of the atmosphere. The profiles of temperature, pressure, and density with altitude will be defined from an altitude of about 100 km to touchdown, from measurements of the atmospherically induced deceleration and directly measured temperatures and pressures, the latter at altitudes below about 20 km. These data will be supplemented by on-board-radar altitudes and, below 8 km, by three component Doppler radar velocities. Winds will be derived from the Doppler velocities and from gyro records of vehicle attitude changes. The planet radius at the landing site, needed to interpret the atmospheric data, will be defined to within a few tenths of a kilometer from the measured acceleration due to gravity after landing. It is expected that temperature will be determined to within about 1 K in the lower atmosphere, and to within a few degrees up to 100 km; pressures to within a few percent; and wind velocities to within about 2 meters/second below 8 km. The design of the sensors is described, with emphasis on acceleration, temperature, and pressure, and the basis for the above error estimates is established.

## 1. Introduction

The two Viking spacecraft launched in August and September of 1975 will reach Mars in mid 1976. They will send landers into the atmosphere to undertake the in situ investigation of many physical features of the planet Mars, and to search for evidence of life there.

The scientific experiments to be performed were described at an earlier stage in the program in a special issue of Icarus (vol. 16, no. 1, Feb. 1972). They include the Entry Science measurements of the planet's bow shock interaction region, ionosphere and upper and lower neutral atmosphere during atmosphere entry and descent, as described in [1]. The present paper will focus on one of these experiments, the measurement of the thermal structure of the atmosphere below 100 km. It will discuss the instruments to be used in more specific terms than was possible in 1972, and summarize further developments in the experiment concepts.

The atmosphere structure experiment has a number of objectives. The primary one is to define the profiles with altitude of temperature, pressure, and density existing at the time and location of entry, accurately and over a broad altitude range extending from roughly 100 km to the surface. In addition, the experiment is expected to establish definitively both the surface pressure and the mean molecular weight of the lower atmosphere, which bear on the presence of bulk quantities of gases other than $CO_2$, and it will seek to obtain information on an increasingly vital subject for the Mars near-surface environment, the winds. Information will be obtained in addition on the terrain profile in the 500 km long swath under the landing

*Space Science Instrumentation* **2** (1976) 381–423. 

path, and on the planetary radius at the landing site, needed to interpret the measured surface pressure. These parameters are to be defined by a synthesis of data read during entry from a number of instruments, including sensors of acceleration, temperature, pressure, altitude, and Doppler velocity.

The problems of achieving these objectives and defining precisely the structure of the atmosphere of Mars are several. In the direct temperature and pressure measurement regime (altitudes below 20 km), the low surface pressure of the atmosphere makes the accurate measurement of $p$ and $T$ a challenge. The nature of the measurement problems, the solutions which have been devised, and the accuracy indicated by tests will be described. Above 20 km altitude, the temperature structure will be deduced from deceleration measurements. (The concepts have been outlined in earlier publications ([1] through [7]), but will be briefly reviewed.) These techniques have been demonstrated in the Earth's atmosphere to be capable of very good accuracy [2]. The critical requirement is that the trajectory within the atmosphere be well established from knowledge of initial conditions and the accelerometry. To deduce the winds in the high speed regime requires a precise definition of the vehicle's orientation history, and knowledge of its aerodynamics. At low altitudes, wind definition will require analysis of the dynamics of the lander on its parachute in a varying wind field.

Before we begin to describe the experiment in detail, it is important that the process by which the instruments were prepared be explained. All the science instruments for the Viking Mission were procured by the spacecraft contractor, Martin Marietta Aerospace Company. The Science Teams formed by NASA Headquarters to investigate the planet were charged with defining the experiment concepts, goals, and approaches, and developing instrument requirements in broad terms. These were translated by the contractor into specifications, and subcontractors were selected to build to these specifications. Subsequently, the Science Teams followed the progress of instrument design, development, and testing, participated in reviews, made recommendations, and raised objections where appropriate, but their overall function would comprise consultation more than direction. Direction of the instrument contractors remained with the spacecraft contractor.

In the case of the Atmosphere Structure instruments, the author established the experiment goals and instrument requirements, outlined possible measurement approaches, participated in design reviews, suggested solutions to problems, and evaluated sensor performance data. Another important function was to hold to high standards of experiment performance as spacecraft and instrument problems arose which often threatened to degrade the experiment. Prototype instruments were tested and evaluated both at contractor facilities and at Ames Research Center, where the able participation of numerous individuals, including R. E. Corridan, M. Gardner, and C. S. James was invaluable. Thus it is evident that many people contributed importantly to the design and development of these instruments, and some of those who played key roles will be cited. At this point in time, it appears that the atmosphere structure instruments which have emerged from this process will

meet experiment goals, in general, although there are areas where they could be improved. The accuracies which we currently expect to realize in the end results will be given.

## 2. Measurement Concepts

### 2.1. Atmosphere structure

Two measurement regimes occur as the vehicle passes downward through the atmosphere: (1) The period of high speed, decelerating flight, in which the entering vehicle loses its initial, near meteoric velocity, and in which the decelerations provide the basis for determining atmospheric state properties. (2) The period of low speed descent, beginning at a flight Mach number of about 2 and extending through the terminal descent phase, when direct sensing of the state properties is possible with only moderate corrections for flight velocity effects.

Figure 1 shows a representative Viking entry into the atmosphere of Mars. Although measurable decelerations occur over the entire altitude range shown, the peak of the deceleration pulse occurs between 60 and 20 km. After the major velocity loss has occurred, the first of two atmosphere temperature sensors is deployed, at 1.1 km/sec (just above 20 km altitude) to begin the direct temperature and pressure sensing phase. Some time later, the parachute is deployed, at nominally 6 km altitude, at which time the lander is extracted (by the parachute drag) from the heat shield, which is jettisoned. The high speed regime of atmospheric reconstruction is continued until this time, so as to provide a 12 to 15 km overlap of the two measurement regimes. At 1.5 km altitude, the parachute is released and retrorockets are fired to set the spacecraft down softly on Mars. All measurements continue in this

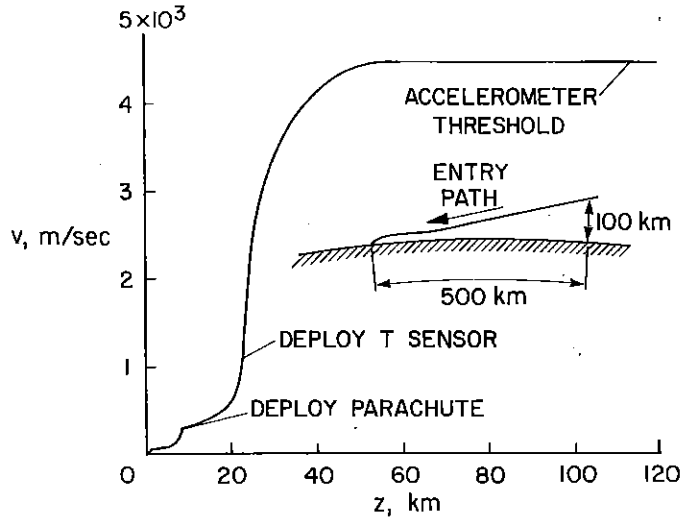


Fig. 1. Viking entry into atmosphere of Mars, representative variation of velocity with altitude.

phase, although there may be some influence by the firing rockets on measured temperature and pressure.

In the high speed regime which comprises 80% of the experiment altitude range, the measurement principle is that atmospheric density is proportional to probe deceleration. Thus

$$\rho = 2Ba_s/V^2, \qquad B = m/C_D A \tag{1}$$

where $B$ is the entry vehicle ballistic coefficient, $m$, its mass, $A$, its frontal area, and $C_D$, its drag coefficient; $a_s$ is aerodynamic deceleration along the flight path, and $V$ is the instantaneous velocity.

The drag coefficient $C_D$ has at this writing been determined in a ballistic range to an accuracy of the order of 1% for simulated entry conditions in a $CO_2$ atmosphere (to be published by Peter Intrieri of Ames Research Center). A preliminary presentation of part of the data (private communication) is given in Figure 2.*

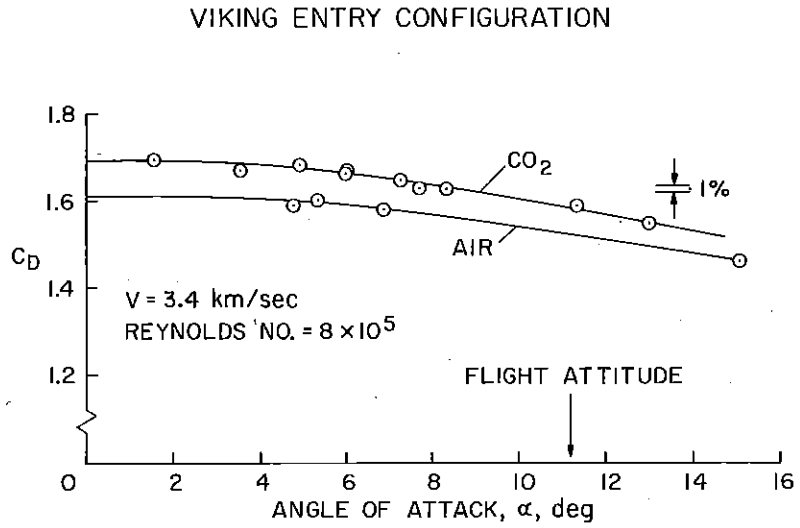


Fig. 2. Drag coefficient, representative data.

The flight velocity $V$ in eq. (1) is accurately tracked from known initial conditions by use of the measured accelerations, and its definition to neccessary accuracy determines the accuracy needed in the accelerometry (order of 1 part in $10^4$). Altitude differences also will be reconstructed from the measured accelerations and the initial conditions (velocity $V_E$ and path angle $\gamma_E$, below horizontal, at entry).

$$\Delta z = -\int_{t_1}^{t_2} (V \sin \gamma)\, dt \tag{2}$$

* For an example of similar data collected for the PAET flight, see [8].

With the assumption of hydrostatic equilibrium, the density profile $\rho(z)$ defined by eqs (1) and (2) yields the pressure profile, $p(z)$.

$$p(z)=\int_z^\infty \rho g \, dz \,. \tag{3}$$

The temperature profile for this altitude regime then follows from the equation of state and the mean molecular weight of the atmospheric gases, $\mu$, obtained from the terminal phase or independent composition measurements.

$$T(z)=\frac{p(z)\mu}{\rho(z)R_u} \,. \tag{4}$$

These are the procedures which were exercised on the Planetary Atmosphere experiments Test probe in the Earth's atmosphere, and shown by comparison with more conventional meteorological data to reproduce the temperature structure accurately, including major gradient reversals and small scale local features [2].

In the lower speed descent, the measurement principle is evident. Sensors exposed to the atmosphere measure the flow recovery temperature and stagnation pressure, which, at low descent speeds, do not differ by much from ambient temperature and pressure, and small corrections can be applied to define precisely the ambient values. The pressure, temperature, and acceleration data are then combined in an analysis (which will not be reviewed here in detail) to obtain descent velocity, altitude, and mean molecular weight of the atmospheric gas mixture [7]. The analysis is based on simultaneous solution of the equation of hydrostatic equilibrium of the atmosphere and the lander descent kinematic equations and yields the following expression for the atmospheric mean molecular weight, $\mu$.

$$\mu=\frac{R_u T}{p}\frac{C_D A}{2mg^2 a_s \sin^2\gamma}\left(\frac{dp}{dt}\right)^2 \tag{5}$$

The symbols have been defined, except for $R_u$, the universal gas constant. If molecular weight is independently known, however, as it likely will be from mass spectrometer measurements on Viking, the vertical flow velocity of the atmosphere $V_v$ may be determined [5] as a function of altitude from

$$V_v=\sqrt{(2R_uT/p\mu)(m/C_DA)a_s}-(R_uT/g\mu p)(dp/dt) \,. \tag{6}$$

## 2.2. Winds

The determination of horizontal wind velocity also has two regimes, in which two distinctly different measurement approaches will be used. In the parachute descent, it will be based on measurements of the lateral velocity relative to the planet surface given by the landing guidance instrument called the Terminal Descent and Landing Radar (TDLR), a Doppler radar. From an analysis of the descent dynamics and aerodynamics, the spacecraft velocity data will be interpreted to define the wind. Lateral accelerations and attitude changes (from guidance system gyros) will be used

to define the departures from equilibrium descent at local wind velocity. This technique is believed to be a powerful one for defining the flow velocities and their profile above the planetary boundary layer in the atmosphere, and should give a definitive but local in situ snapshot of the instantaneous planetary wind at the two landings.

At retrorocket ignition, when the parachute is jettisoned, the mode of spacecraft operation changes. Then the rockets are used to bring the horizontal and vertical components of land velocity to zero at a point a few meters above the surface. At this time, the lander attitude required to enable the retrorocket to counteract the wind force becomes the measure of the horizontal wind. Although data from this phase will be examined, no requirements were imposed on the lander design to assure a successful wind measurement for this phase (below 1.5 km), and the attitude angles required to overcome the wind are quite small (e.g., 0.4° for a 50 m/s wind). Thus there is no present certainty that the retrorocket phase will yield satisfactory wind data.

In the upper atmosphere, winds can in principle be detected from their effect on the lander resultant velocity relative to the atmosphere. When the resultant velocity vector is rotated by the presence of wind, the lander itself rotates the same amount (after oscillations are damped) to maintain its trim aerodynamic alignment. This rotation is detected by the gyroscopes in the guidance system, and can be used to infer the wind.* Winds are detectable both in-plane and across-plane to the lander flightpath, but if they are exactly co-linear with the flight direction, no rotation of the apparent "relative wind" direction results. Hence, when the lander approaches nearly horizontal flight (as it does between 25 and 30 km altitude), the measurement loses sensitivity to in-plane horizontal winds. There is also an ambiguity between trim angle errors and wind. For example, a sustained sideslip angle cannot be differentiated from a sustained cross-path wind. However, a sustained aerodynamic trim angle has a "signature", namely a constant or nearly constant difference in attitude from that expected, whereas a wind profile to produce this same angular deviation would have to be matched to the lander velocity as a function of time, and thus is highly improbable. Hence, significant measurements of the planetary wind velocities at high altitudes are expected to result from use of these procedures even in the presence of aerodynamic trim.

### 2.3. Terrain and planetary radius

The Viking Lander carries a radar altimeter, which measures distance to the nearest terrain. The altimeter will be used in the atmosphere structure experiment to establish altitudes $z_{RA}$ for the state property profiles, but since it reads to the nearest terrain, it is sensitive to terrain features. It is furthermore redundant to the determination of altitude above impact from the accelerometers, pressure, and temperature sensors, eq (2) and reference [7]. By comparison of the two independent

* This concept is due to R. Blanchard of Langley Research Center and J. Findlay of Analytical Mechanics Associates.

altitude histories, the terrain profile will be defined (except during radar altimeter blackout*) as a function of location along the entry path

$$z_{\text{terrain}} = z_{RA} - z_{a,p,T} \tag{7}$$

Referenced level for the terrain data will be the altitude of the landing site, to which $z_{a,p,T}$ is referenced.

Absolute radius of the planet at the landing site will be determined from readings of the local acceleration due to gravity $g$ by the three-axis accelerometer after landing, through the gravitational equation

$$R = \sqrt{GM/g} \tag{8}$$

where $GM$ is the product of the universal gravitational constant and the planet's mass, measured by the Mariner 4 and 6 flyby spacecraft to be 42828.2 and 42828.3 $km^3/sec^2$, respectively [9].** Correction for local gravitational anomalies (order of 500 ppm) should be at least roughly possible from Mariner 9 data [10][11]. A measurement of $g$ accurate to 1 part in $10^4$ will yield the planetary radius within 170 m, while definition to 1 part in $10^5$ will give radius within 17 m. These two values bracket the expected limits on instrument performance in the presence of the test, launch, cruise, and entry environments. Telemetry resolution of $1.1 \times 10^{-5}$ in $g$ is achieved by integration of indicated velocity increments for the planned period of 5 minutes after landing.

From the viewpoint of the atmosphere structure determination, the importance of the landing site radius is its influence on the surface pressure, and subsequent interpretations of the measured pressure. The pressure varies with altitude by a factor of $e$ per scale height (nominally 12 km). For 120 m altitude uncertainty, then, the equivalent uncertainty in pressure is about 1%. We have worked to control the uncertainty due to planetary radius in interpreting the measurements to about this level.

## 3. Instruments

### 3.1. General Arrangement

The Viking entry vehicle and lander, as they will be configured during the high velocity entry and parachute descent phases, are shown schematically in Figure 3.

* Period during which the altimeter signal does not escape through the ionized bow shock envelope of the entry vehicle.

** Equation 8, corrected for centrifugal force due to a planetary rotation, becomes

$$g = GM/R^2 - (\omega \cos \varphi)^2 R$$

where $\varphi$ is landing site latitude. The correction term at 20° latitude is 0.4% of the gravitational acceleration, and may be incorporated by iteration. Landing site latitude must be known to within 0.2° for 17 m uncertainty in $R$, and to within 2° for 170 m uncertainty. Present estimates are that radio tracking will define the latitude after landing to within 0.1°.

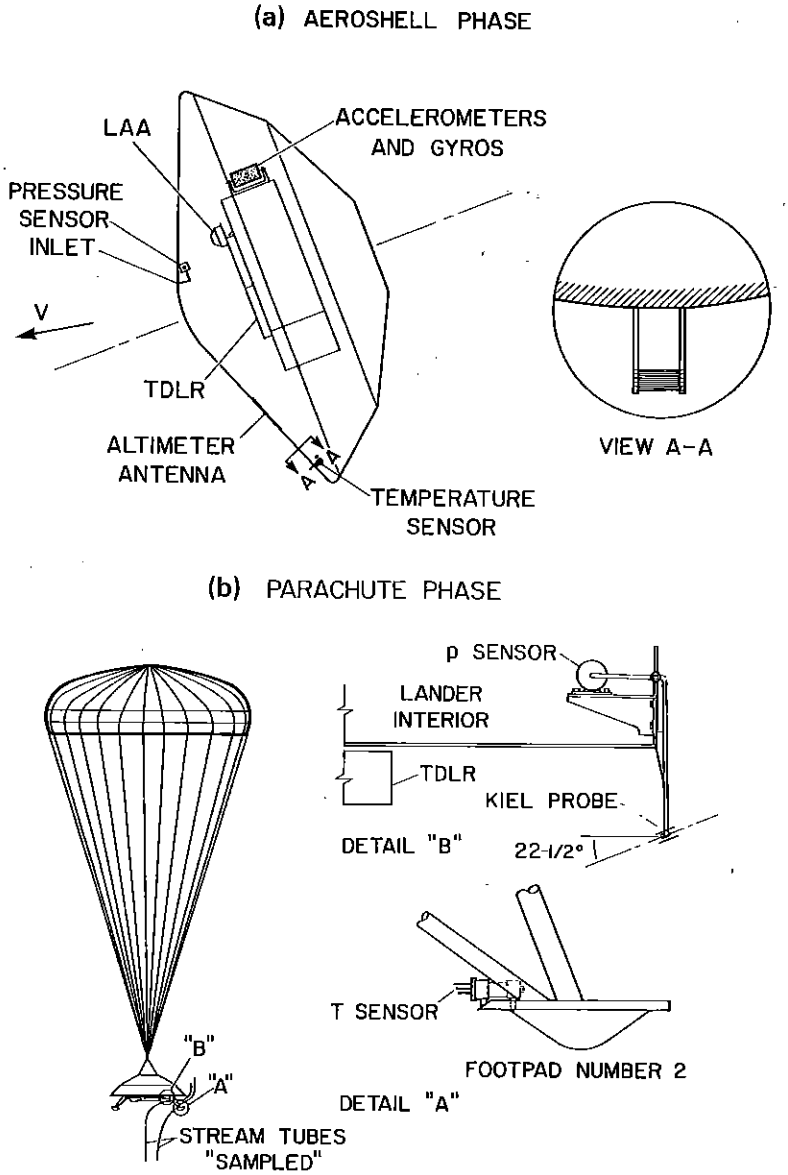


Fig. 3. Locations of the atmosphere structure instruments on the Viking entry vehicle and lander.

The conical forward face of the entry vehicle, called the aeroshell, provides the lander with heat protection and stability, and at its trim angle of attack of $-11.2°$, develops aerodynamic lift and drag to fly the prescribed trajectory during the high velocity entry. It is jettisoned when the parachute is deployed, to expose the lower surface of the lander, the Doppler radar (TDLR) antenna, and the terminal descent engines, which are 3 groups of multiple small nozzle engines mounted on the lander

sides intermediate between the landing legs. The legs are deployed within a few seconds after parachute deployment.

As is indicated schematically in Figure 3, most of the atmosphere structure instruments are mounted in the lander and retained when the aeroshell is released. These include the accelerometers, one pressure and one temperature sensor, the radar altimeter electronics, and the TDLR. There are two altimeter antennas, however, one on the aeroshell and one on the lander, the latter designated LAA in figure 3(a).

Since temperature measurements are made before and during the parachute phase, and stagnation pressure measurements are made throughout the entry, two sets of $T$ and $p$ sensors are provided, one on the aeroshell and one on the lander. The aeroshell pressure sensor port is in the stagnation region of the entry vehicle at its trim angle of attack while the temperature sensor was located on the vehicle front face on the leeward side near the aeroshell outer edge to maximize the mass flow rate of atmospheric gases about the sensing element. The sensor is protected from the severe aerodynamic heating at entry by being retracted in its housing, behind the heat shield. At 1.1 km/sec, it is deployed by a spring-driven mechanism which first ejects a plug of heat shield material and extends the sensor to a position above the vehicle surface boundary layer.

The temperature sensor on the lander is located on the upper, inboard edge of footpad 2. When this landing leg is extended, the sensor elements are normal to the local streamlines in a region of vigorous flow moving at approximately the descent velocity. The sampled stream tube is unheated by any possible contact with the lander.

The lander pressure sensor is ported through a Kiel probe, a ducted pitot probe which is insensitive to angle of attack, located just below and off the edge of the lander body. The Kiel probe axis is approximately parallel to the theoretical streamline direction at that location.

### 3.2. Accelerometers

The accelerometers are a key instrument, used in all phases of the experiment, and for a number of independent purposes. Four accelerometers will be carried on each lander, two aligned parallel to the vehicle axis of symmetry, the $x$ axis, and the other two in orthogonal directions, parallel to the $y$ and $z$ axes. The sensors are housed in the guidance and control system inertial reference unit (IRU), and are used jointly for guidance and experiment purposes.

*Description.* The Viking acceleration sensors are derived from standard, high performance, guidance accelerometers. As indicated schematically in Figure 4, they sense acceleration by measuring the electromagnetic restraint needed to hold a test mass in a precise null position along the sensing axis. The test mass is supported and constrained in the other two directions by thin flexures. The restoring force is provided by a current flowing in a coil mounted in the test mass, which reacts against

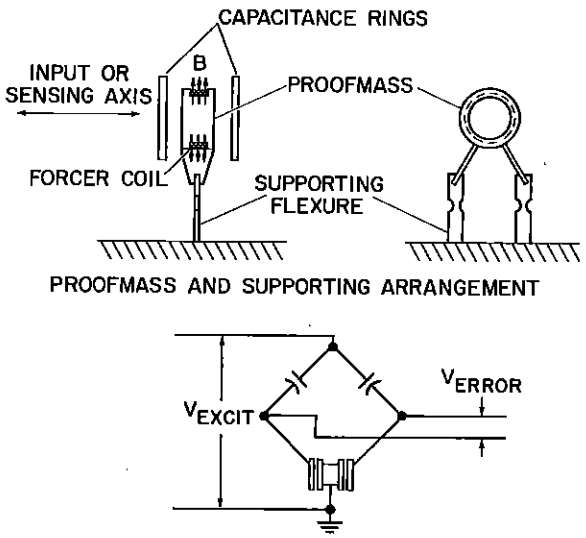


Fig. 4. Viking acceleration sensor (Bell Model IX).

the permanent magnetic field B in the sensor. Deviations from null of test mass position are detected by capacitive sensing, as shown schematically, and the current to maintain null is servo controlled by the error signal in a feedback loop. The nulling current is the measure of the acceleration. With suitable current scale factors, the sensors detect and measure accelerations less than $10^{-5}$ m/s$^2$ (10 $\mu$m/s$^2$). Output is highly linear, and nominal long term scale factor and bias stabilities are $10^{-4}$ and 1 mm/s$^2$ (100 $\mu$g), respectively. These sensors were provided by Bell Aerospace Company, and are designated Bell Model IX.

*Electronics and Data System.* The accelerometers, together with a three-axis set of gyroscopes, were integrated into the Inertial Reference Unit (IRU) by Hamilton Standard Division of United Aircraft Company, the IRU subcontractor. Hamilton Standard digital electronics were employed, in which the nulling current is a continuous 1 kHz square wave, with equal positive and negative amplitudes. The time share of the positive and negative current periods is, however, unequal under acceleration, and is adjusted to provide the required average nulling current. This unsymmetrical pulse wave pattern is electronically compared with a symmetrical 1 kHz square wave and the difference current is integrated to generate velocity pulses, nominally 1.22 cm/s in the $x$ axis and 0.305 cm/s in the $y$ and $z$ axes. The accumulated number of velocity pulses, properly resolved directionally, is the velocity change from the entry velocity $V_E$, with cumulative resolution to within 1 pulse. (The importance of this consideration is evident from Eq. (1).) One of the axial sensors will be sampled by the spacecraft in just this way. The accumulated number

of pulses, read in a single 24 bit word, will be read at 1 second intervals. The remaining triad of sensors will be sampled at 0.1 second intervals in 10 bit words to read the velocity change in the sampling interval. The 10 bit word can accommodate a peak deceleration in the $x$ direction of 125 m/s$^2$, which accommodates with some margin the peak deceleration in the nominal entry case, 73.3 m/s$^2$.

*Sensor Accuracy in the Test Program.* The specifications on accuracy were as follows: Scale factor stability, within 0.05% for a period of three years after acceptance test, through all test and operating environments. Scale factor knowledge, within 0.02%, for the same period. Scale factor short term repeatability, within 0.003%, within 24 hours. Bias stability, within 1.8 mm/s$^2$, through all environments from lander separation from the orbiter through landing and 10 days' operation on the planet surface.* Sensor acceleration threshold was specified to be 0.05 mm/s$^2$. Cross axis sensitivity was limited to 0.5 mm/s$^2$ per g.

Test results obtained with the prototype IRU, called the Design and Development Unit, shows scale factor stability generally (but not always) within 0.05% through the test program of simulated environments, including sterilization cycles, pyro shock, random vibration, landing shock, and entry and surface thermal environments, over a two month period. Run to run repeatability and cross axis sensitivity were within specifications. Bias stability better than that required, within 0.8 mm/s$^2$, was demonstrated through this test period. However, in a simple ten hour bias stability test, surprisingly, bias shifts as large as 0.7 mm/s$^2$ were seen, corresponding to maximum planetary radius errors of 0.3 km. Generally speaking, it appears that the instruments will perform within specification, except possibly in scale factor knowledge, where they could slightly exceed specification.

*Location and Alignment.* The original experiment specification called for the accelerometers to be located near the entry vehicle center of gravity, with the primary axial sensor test mass on the c.g. The Viking contractor encountered difficulties in meeting this requirement, because of IRU thermal control problems, and located the instrument outside the lander body, centered on a point with nominal coordinates ($x$, $y$, $z$) of 4, 22, −98 cm. In this location, the accelerometers will respond to some components of the angular acceleration and angular velocity of the lander. The lander is, however, rate-limited during entry to 1 deg/sec about its aerodynamic trim attitude by a reaction control system. A careful simulation study of the system dynamics (performed by Paul Kusinitz at Martin Marietta Aerospace Company) showed that the angular inputs to the sensors under these conditions would be negligible. Furthermore, the gyro data will permit corrections for angular

* This bias error leads to a velocity error of 0.36 m/s in a 200 second integration period typical of the time from the final zero calibration prior to first sensing of aerodynamic deceleration to deployment of the low speed sensors. In this short time period, an error of this size is very unlikely. In the 5 minute period of landed operation, if present, it would yield an error in planetary radius at the landing site approaching 0.8 km.

inputs if conditions exceeding those calculated should occur. For the purposes of making such corrections, the centroid of each sensor test mass relative to the entry vehicle center of gravity was determined within 1.3 mm.

The sensor alignments required were dictated by the accuracy goals and the aerodynamic force levels expected. By far the largest force is in the axial direction; the normal force in the $xz$ plane (lift plane) is 0.016 as great, and that in the cross path plane is nominally zero. To measure the axial force to within $10^{-4}$ (0.01%) of its correct value (and thus match the sensor nominal capability), the axial sensors need only be aligned within 0.014 radian of the vehicle axial direction, or 0.8°. The $y$ and $z$ axis sensors, however, to avoid sensing a component of the axial force larger than 0.1 of the expected force in the lift plane, should be aligned within 0.00156 radians, or 5.4 minutes of arc. With this alignment, the readings in $a_z$ and $a_y$ would be in substantial fractional error (10%), and require correction, so knowledge of alignment about ten times better was specified.

The $y$ and $z$ axis accelerations will be used in two ways: (1) To define the angles of attack and sideslip during entry, which may differ from those expected on the basis of ground facility measurements. (2) To reconstruct the curvature of the flightpath in the vertical and horizontal planes.

The specification on alignment of the $y$ and $z$ axis sensors given the IRU contractor was 6 arc minutes, with knowledge of alignment specified to be within 0.5 arc minutes. Stability of alignment within 2 arc minutes for a three year period was also required. At the Critical Design Review, in August 1973, the contractor indicated ability to align the sensors within 3 arc minutes, and to know the alignment within 0.23 arc minutes.

Alignment of the sensors to the spacecraft axes also depends on aligning the IRU unit to the spacecraft. A procedure to achieve alignment within 15 arc minutes (0.25°), with knowledge to within 0.5 arc minutes was devised. However, the IRU is mounted on shock mounts, to isolate it from nearby pyro shock events which could impair operation of the gyros. The effect of shock-mounting on alignment stability was studied by Hamilton Standard. Shock mounts were tested under load through sterilization cycles. The measured creep effects in the mounts would cause a three year alignment error of 1.4 arc minutes, $3\sigma$, since only differential creep will cause rotation of the IRU. In fact, the most damaging rotation, about the $y$ axis, requires a highly improbable asymmetric distortion of the two upper mounts relative to the lower two, in directions perpendicular to the mount axes.

Structural deformations of the lander also could affect alignment. Deformations associated with aerodynamic loading and thermal stress were investigated, and found to be within the alignment specifications.

*Calibration.* Calibrations to establish scale factor and non-linearity of the flight sensors were performed in the Earth's gravitational field at accelerations between 0 and 1 g, or $-1$ to $+1$ g. (The operating ranges of the instruments are 0 to 20 g, $x$ axis, and $-5$ to $+5$ g, $y$ and $z$ axes.) In calibration, the instrument is mounted in a

precision indexing head and rotated to several orientations with respect to the vertical in order to vary the input force along the sensing axis. The sensor manufacturer (Bell Aerospace) and the Viking contractor (Martin Marietta Aerospace) have extensive experience which indicates that, because of an unusual degree of sensor linearity, calibrations obtained in this way can be reliably extended to much higher levels of acceleration. This has been demonstrated in the past by calibrations to much higher acceleration levels on a precision centrifuge.*

Additional calibrations were made of the servo-loop electronics in bench tests to establish accuracy and linearity over the full use range. Tests were also performed to determine the "break-away torque" and full range freedom of movement of the test masses.

Nonlinearity of the sensors was limited by specification to the order of 100 ppm. In tests of the Design and Development sensors between 0.5 and 1.0 g, it was found to be between 15 and 40 ppm. While these nonlinearities are small, they were established for individual flight sensors and the coefficients will be used in interpreting the data.

*Frequency Response.* The frequencies at which the accelerometers are required to have accurate response range from 0.07 Hz, which characterizes the principal deceleration pulse, to 1 Hz, which is close to the peak frequency of the aerodynamic pitching oscillation. Since the sensor test mass is servo-loop constrained, the servo-loop characteristics determine the frequency response. An analysis and a numerical simulation of the loop characteristics performed at Hamilton Standard showed that at 1 Hz, the amplitude response error was 1% of amplitude, and the phase error, 0.22°. At 0.07 Hz, the amplitude error calculated was 0.023%, and the phase error was negligible. A nonlinear simulation of the $y$ and $z$ axis sensor response to a 2 g, 2 Hz sine wave (an input well in excess of any expected, both in frequency and amplitude) showed a maximum amplitude error of 15% or 0.3 g. This error was a result of displacement of the signal relative to the input, that is, response exceeded input on the negative half wave, but fell short of input on the positive half wave. The validity and significance of this simulation result is not presently clear. It does not agree with the linearized analytical error predicted at 2 Hz which indicates an amplitude error of 3.3%, and a phase shift of 0.65°. This higher frequency response error applies only to the oscillating ripple which is superimposed onto the principal deceleration pulse as a result of pitching and yawing motions. The latter are rate limited to small amplitude by the reaction control system. Hence, the frequency response does not appear to be a significant error source, but it will be reexamined in relation to the flight data when they are obtained.

* The author argued that precision centrifuge calibration should be performed with the flight instruments as a matter of good practice. However, cost considerations and the argument that past experience showed it to be unnecessary prevailed. No centrifuge calibrations were performed. Thus, the instruments were neither calibrated nor functionally tested, in an end-to-end sense, for accelerations beyond 1 g.

### 3.3. Temperature sensors

*Approach.* To measure the temperature of the low density atmosphere of Mars accurately, a sensor must exchange heat rapidly with the surrounding gas, while heat transfer by radiation and conduction from extraneous sources is kept small. Quantitatively, at equilibrium, the temperature error $\delta T$ due to a radiative or conductive heat input or loss rate $q$ (watts) is governed by $hA\,\delta T = q$, where $A$ ($cm^2$) is the wetted area for forced convective heat exchange with the atmosphere, and $h(W/cm^2\,K)$ is the convective heat transfer coefficient. If $q < hA$, $\delta T$ will be small. However, $h$ is proportional to $\sqrt{\rho V}$, where $\rho$ is ambient gas density and $V$ is the fluid velocity driving the forced convection. Therefore, two things are evident: (1) For gas densities less than 0.01 amagat, typical of Mars, convective heat exchange at a given flow velocity will be less than 0.1 that under Earth sea level conditions. (2) The effect of low gas density will be counterbalanced by the fairly high velocities of descent of the Viking lander, provided that the sensor is located in a region of high local gas velocity.

Considerations of this kind, made quantitative, plus the consideration of fast response required to follow the rapidly varying recovery temperature early in the deployment of the aeroshell phase sensor, governed the selection of the Viking temperature sensor. Designs with sensors bonded to relatively thick supporting structures, or enclosed in protective housings, were eliminated from consideration because of high heat capacity, low convective heating rate, high conductive inputs, or precooling of the atmospheric sample by the housing. The sensor which was selected is a set of fine wire, butt welded thermocouples, 0.127 mm in diameter, exposed directly to the local atmosphere and oriented normal to the streamlines. Wire lengths about 184 times the diameter were provided to limit conduction errors. The fine wire diameter favors quick response. Radiative exchange with the surroundings was limited by use of materials of relatively low emissivity. Furthermore, the sensors are supported from small diameter, thin-walled tubes (2.4 mm o.d., 0.25 mm wall thickness) which themselves have small thermal lag. Thus, the temperature difference available to drive conduction errors is minimized. The posts and leads going to the cold junctions in the sensor electronics package were made of the thermocouple materials to avoid the introduction of additional thermoelectric junctions. A platinum resistance thermometer within each sensor housing monitors the cold junction temperature.

Errors due to convective heat transfer from the spacecraft to gas which passes over the sensor were entirely avoided by placing the sensors outside of the vehicle boundary layer, since the vehicle does not influence the atmospheric total temperature outside its own boundary layer except by radiation (which can be ignored at expected gas densities and temperatures).

Since the sensor is in rapid motion relative to the atmosphere – typically from 70 m/sec to 1100 m/sec – the convective heat exchange is vigorous. However, the high velocities also increase the magnitude of corrections for effects of flow velocity.

The temperature sensed, called in fluid mechanics the flow recovery temperature, $T_r$, is defined (for a gas of constant $c_p$) by

$$T_r = T_\infty + rV^2/2c_p \tag{9}$$

where $T_\infty$ is the ambient atmospheric temperature, $c_p$ is the specific heat of the atmospheric gas mixture, and $r$ is the recovery factor – the fraction of the flow kinetic energy which is recovered as thermal energy in the sensor. The parameters in the kinetic temperature term are known – the velocity from the accelerator data and the trajectory reconstruction; the specific heat from the atmospheric composition; and the recovery factor from ground facility tests.* Composition of the atmosphere will be determined by two mass spectrometers on Viking ([1] and [12]) and will also be grossly evaluated from the mean molecular weight as determined from Eq. (5).

The magnitude of the kinetic temperature difference $T_r - T_\infty$ for the parachute descent is from 2 to 30 K. It will be shown that for these conditions, error in the correction to the measured temperature should be hundredths to tenths of a degree. For the higher velocities early in the aeroshell phase, the dynamic temperature increment will be initially larger than the ambient temperature and it must therefore be very accurately evaluated to preserve accuracy in the ambient temperature. We will discuss the accuracy which we think can be realized in this phase.

*Description of Flight Sensors.* The two atmospheric temperature sensors on each Viking entry vehicle were an extension of the design of similar sensors used on the Planetary Atmosphere Experiments Test vehicle (PAET) in the Earth's atmosphere [2, 13]. The Viking sensors were designed and developed by a team headed by Dr. Robert Dennen from the Space Science Department of Martin Marietta Aerospace Corp., Denver Division. Mr. Ludwig Wolfert was largely responsible for the electronic design, Mr. William O'Connor and Mr. Dale Shields for the mechanical design, and Dr. Wayne Simon for analysis of aerodynamic aspects of the design. Drawings and photographs of the aeroshell and parachute phase instruments are given in Figures 5 and 6.

Each sensor has three sets of support posts (Fig. 5) with three thermocouples in parallel between each pair of posts. The redundant thermocouples in parallel provide insurance against breakage which could result from launch or entry vibration, deployment shocks, heat shield particle impacts, etc. If only one thermocouple in each row were to survive, the sensor would return its data, and there is also an operating mode if only one thermocouple in the first row survives. The redundancy was provided in recognition of the fragile nature of fine wire thermocouples. With the present design, however, (see below) the sensors have successfully withstood repeated qualification and acceptance test environments without failure.

* Measurements of $r$ in $CO_2$ at a gas temperature of 300 K have been completed, with Viking sensors at simulated Viking entry conditions. A representative value is 0.84 for a sensor wire diameter Reynolds number of 15. These measurements will be the subject of a separate publication.

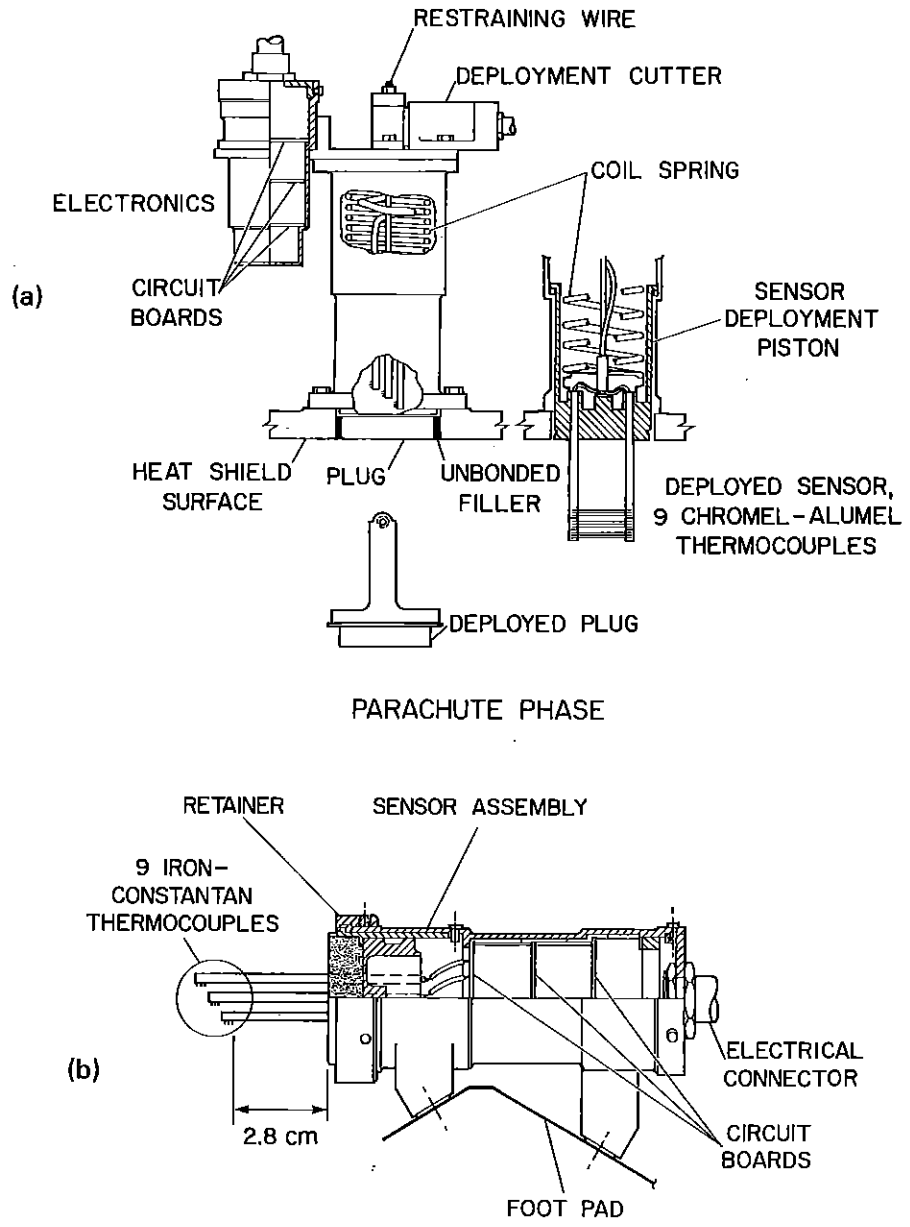


Fig. 5. Viking temperature sensors, schematic drawings: (a) Aeroshell phase sensor; (b) Parachute phase sensor.

The three rows of thermocouples are connected in series, as shown in Figure 7, to build up full range outputs of 0 to 40 mv without amplification. (This rather basic feature of the design was due to Mr. Wolfert and Dr. Dennen.) Since the sensors are arranged in a line along the flow direction, the sensor wires were staggered in

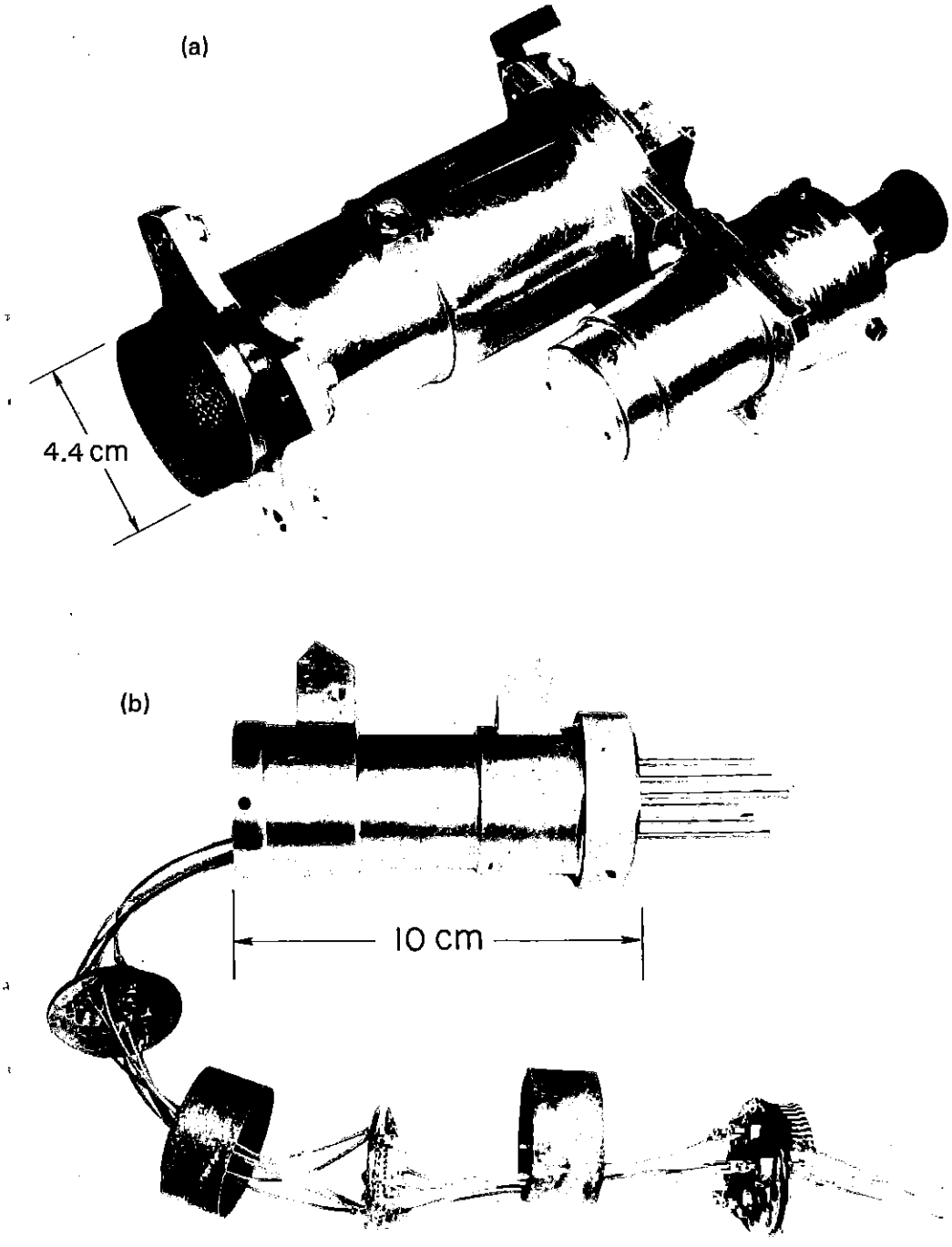


Fig. 6. Photographs of the temperature sensors: (a) Aeroshell phase sensor retracted in its case; (b) Parachute phase sensor.

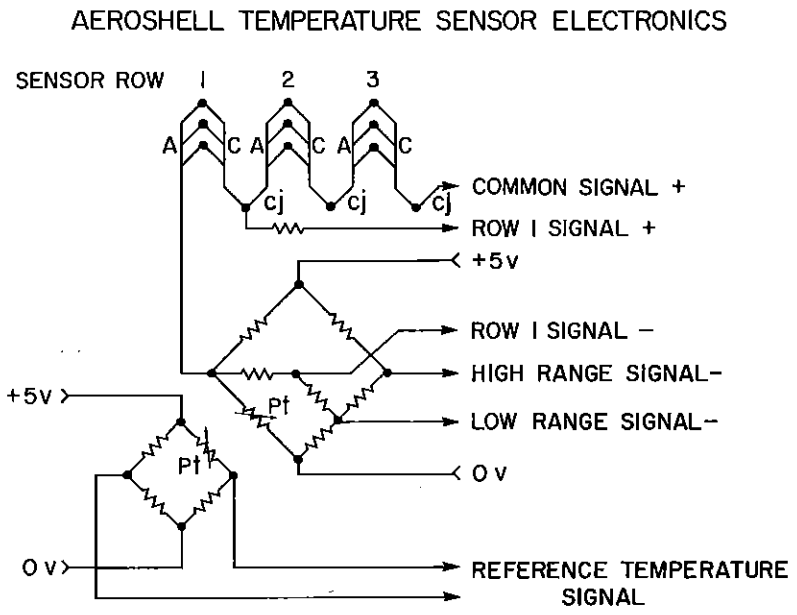


Fig. 7. Aeroshell temperature sensor circuit diagram.

distance from the mounting surface, by 0.76 mm within each set, and by 1.52 mm between sets, to prevent interference between wires and between rows. Those in the rear are thus not in the viscous wake of more forward wires.

The temperature range of the aeroshell sensor was chosen to encompass the recovery temperature at deployment as well as the much lower atmospheric temperatures seen as the vehicle slows down. Thus, it has two ranges, 100 to 460 K, and 440 to 750 K. In the parachute phase, a single range suffices, 100 to 400 K. The thermocouple materials selected were, for the aeroshell sensor, chromel and alumel; and for the parachute phase, iron and constantan.

The primary function of the very simple sensor electronics indicated in Figure 7 is to shift the output to 0 mv at the lower end of each measuring range, by means of the resistance network shown beneath the sensors and the excitation voltage (5 v) applied to the bridge. In addition, the row 1 signal is presented separately as a single range, from 90 to 750 K with a signal span of 25 mv.

The platinum resistor in the lower leg of the network provides automatic cold junction temperature compensation to within 6 °C in output signal for cold junction temperatures over a range of 115, from 220 to 335 K. The cold junction temperature read by the separate platinum resistance thermometer, shown at the lower left, will be transmitted to Earth to correct these readings and provide the ultimate reference for the temperature measurements. This thermometer is located close to the thermocouple cold junction within the sensor electronics packages shown in Fig. 5. Root-sum-square errors contributed by the electronics, due to shifts in the resistance values in the network and in the excitation voltage, were conservatively estimated to

be less than about 1.3° in the aeroshell phase, and 1.0° in the parachute phase, for an electronics temperature near 273 K.

The sensor output signals will be sampled once per second in the aeroshell phase and twice per second in the parachute descent by the lander data acquisition and processor unit (DAPU). The DAPU provides analog to digital conversion. It also supplies the excitation voltage (5 v), the exact value of which is monitored and transmitted as part of the spacecraft engineering data. The 8-bit temperature telemetry words will give resolution of nominally 1.2° to 1.4 °C, and error in a single $A$ to $D$ conversion can be as large as the resolution element.

Deployment of the aeroshell sensor is a fairly critical requirement. It is made necessary by the high flow recovery temperatures which occur early in the entry (up to about 4000 K), more than enough to melt the thermocouples. During this and all prior mission phases, the sensor is within its housing, held in place by a restraining wire against the compressed coil spring. At deployment, the restraining wire is cut by a pyrotechnic cutter, and the spring deploys the sensor. The piston on which the sensor is mounted simultaneously ejects a plug of heat shield material held on supporting arms, very carefully installed to insure that it will be retained until it is ejected by the force of the spring. When the heat shield plug emerges, its supporting arms permit it to rotate only in the downwind direction, so that it will depart without breaking thermocouple wires. This system was tested many times, once in a high temperature arc jet flow, where both the heat shield thermal degradation and aerodynamic forces present at deployment were approximately simulated. In the tests, it was observed that the stopping shock of the piston at the end of the deployment stroke was rather severe. It sets the sensor wires into many cycles of oscillation of about 1 mm amplitude, but it did not break thermocouples. The deployment mechanism was shown to work reliably and without damage to the sensor.

In early designs, wires were broken during vibration and shock tests. The breaks were either at the thermocouple junction or at the welds onto the support posts. The sensor wires at that time were straight, but were welded with some excess length between the posts so that they would not be broken by post vibrations. Additional steps were taken: (1) The sensing wires were coiled into helical springs by turning them around a 0.35 mm rod. The spring was stretched to a pitch of roughly 2 mm before welding. It could then stretch under load without breaking. (2) A single bead of silicone rubber adhesive was applied where the wires contact the support posts, to support the wires at the weld points against flexing. With these changes, the sensors have withstood all of the test vibration and shock environments, including the aeroshell sensor deployment shock and (for the parachute phase) landing leg deployment shock (1900 g's).

*Calibration.* Reprensentative calibration data for the temperature sensors are shown in Figure 8. The calibrations were performed in a stirred, temperature-controlled bath, in several different fluids for different temperature ranges: A

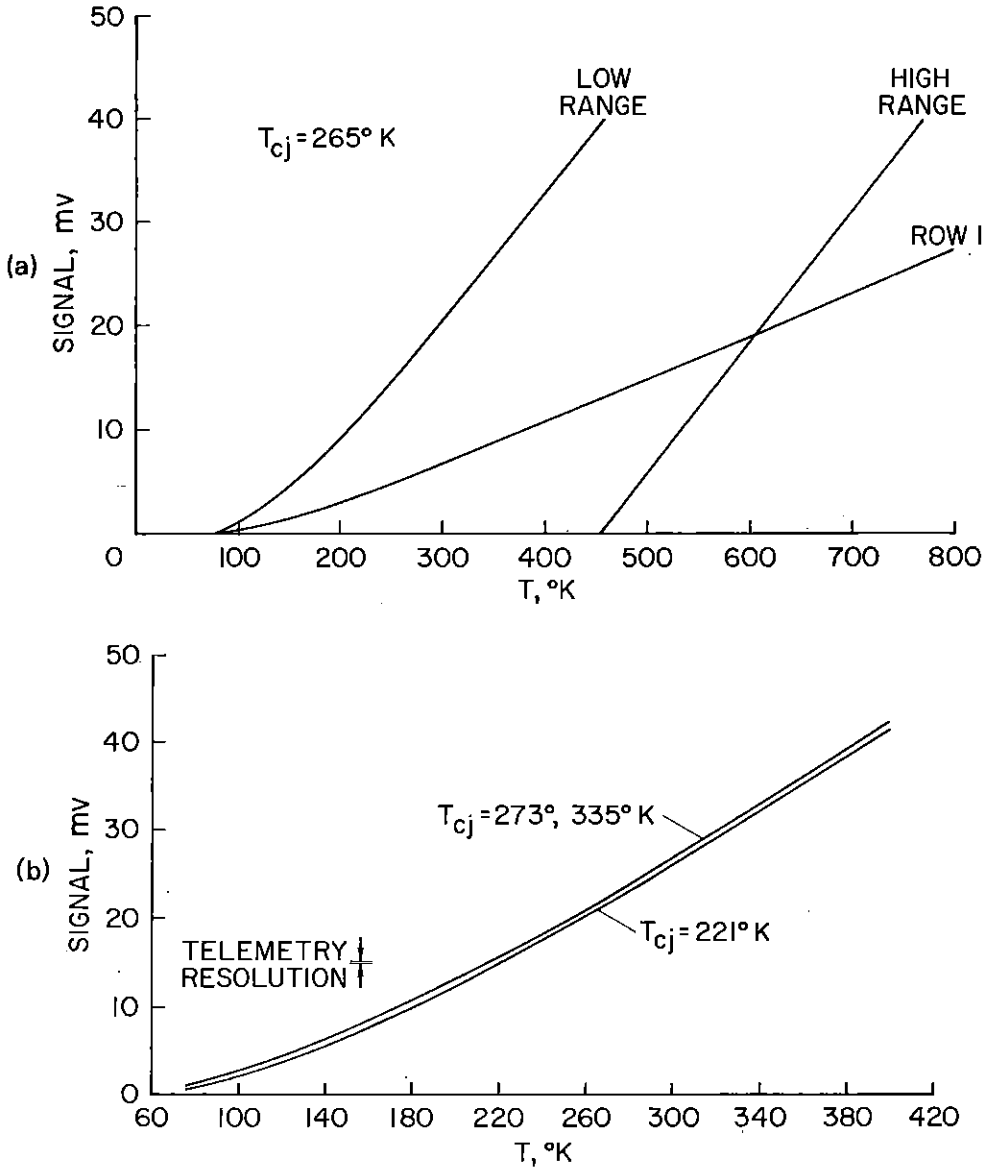


Fig. 8. Temperature sensor calibrations: (a) Aeroshell sensor; (b) Parachute phase sensor.

polyphenyl ether (Monsanto OS 124) was used at the highest temperature point, 750 K; a silicone oil (DS 704), at intermediate temperatures from 330 to 600 K; Freon 12 and Fluorinert at temperatures from 135 to 273 K at which the other fluids become excessively viscous or solid; and liquid nitrogen at its boiling point, 77.4 K. The temperature standard was a secondary standard resistance thermometer, calibrated at the NBS. The sensor posts and thermocouples were dipped into the bath to a

depth where the topmost thermocouple was 1.27 cm below the liquid surface. The sensor was allowed to attain a steady reading and read together with the standard. Six temperature points were used between 77 and 750 K for the aeroshell phase sensors, and six between 77 and 400 K for the parachute phase sensors. Electronics housing temperatures were separately controlled, and were stabilized at three temperatures from 218 to 311 K for each bath temperature. After calibration, the sensors were carefully cleaned in organic solvents to remove all visible traces of the bath fluids.

Statistical analysis of the calibration data taken showed that the probable error of calibration (1 $\sigma$) ranged from 0.06° to 0.7°. Smallest uncertainties ($\sim 0.1°$) occurred in the most probable use range of the parachute phase sensors (135 K to 273 K); the largest, at the high and low temperature extremes.

To guide interpolation between the calibration points, standard charts for thermocouples of these materials, and calibrations with closer-spaced temperatures performed at Ames Research Center with the design and development (DD) sensor will be used. The DD sensor is nominally identical to the flight sensors. Thermocouple wire for the DD and flight sensors came from the same spools, and these spools were certified by the supplier to be in conformance with standard thermocouple emf tables within 1 °C to 530 K. Deviations of this material lot from the standard emf tables were given.

The degree to which the resistance network thermal compensation reduces calibrations to a single curve for the range of cold junction temperatures tested (and expected) may be seen in Figure 8(b).

*Measurement Errors.* In addition to errors due to calibration and spacecraft electronics, there are the measurement error sources indicated earlier, which are associated with finite response time, support conduction, emission and absorption of radiation, and with the kinetic temperature correction. These error sources have been analyzed in considerable detail, and in the following paragraphs, estimates will be presented of their individual magnitudes.

Response time was a governing consideration in the selection of thermocouple wire diameter. It depends on the diameter $d$, wire density $\rho_w$, and heat capacity $c_w$, gas viscosity $\mu_s$, and conductivity $k_s$ evaluated at the stagnation temperature, and fluid mass flow per unit area over the sensor $\rho V$ according to

$$\tau = \frac{c_w \rho_w d^{3/2}}{2 f k_s} \sqrt{\frac{\mu_s}{\rho V}} \tag{10}$$

where $f$ is a factor to represent the variation of dimensionless heat transfer coefficient (Nusselt number) with local Mach number* ($f = 1$ for $M = 0$). For the selected wire diameter, the longest response time during parachute descent in the Viking mean model atmosphere is 0.86 seconds, during which the lander descends nominally 50 meters. For a temperature lapse rate in Mars atmosphere of 4 K/km, the change in

* For an implicit example of this dependence, see [14].

ambient temperature in the maximum response time is thus of the order of 0.2°, and the sensor is expected to follow ambient temperature within about this lag. (This approximation is exact, at equilibrium, for a linear variation of $T_r$ with time.)

In the aeroshell phase, a shorter response time is needed because of the rapid variation of kinetic temperature with time soon after the sensor is deployed, which may be as great at 15°/sec. The response time was therefore required by specification to be less than 0.3 second at deployment, and in one example trajectory which has been analyzed in detail, it was actually 0.2 second. The low response time obtained in this phase, as compared with the parachute phase, results from the higher mass flow rates and higher stagnation temperature, which increases the gas conductivity. The estimated equilibrium lag errors given by $\delta T = (dT_r/dt)\tau(t)$ are given in Figure 9 by

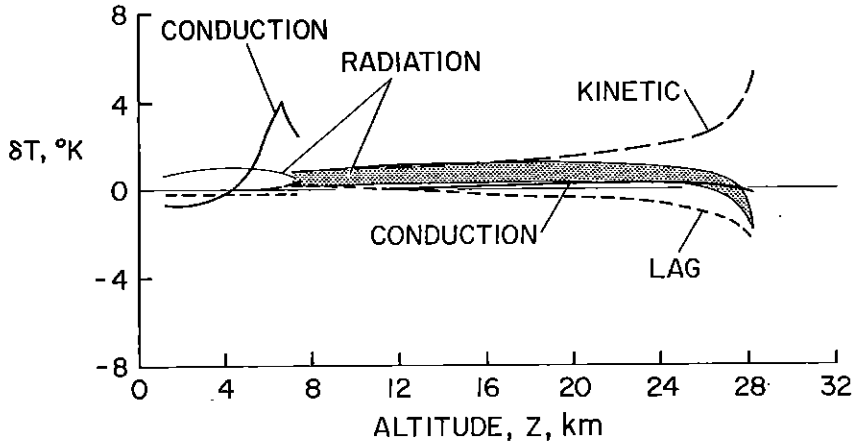


Fig. 9. Estimated measurement errors in temperature for the direct temperature sensing regime.

the curves labeled "lag". For the trajectory and atmosphere modeled in this example, the lag error is initially −2° in the aeroshell phase, but drops in magnitude to the level of a few tenths of a degree below an altitude of about 22 km, due to the reduction in the recovery temperature rate. Lag errors will be correctable post-flight from the record of the recovery temperature rate and knowledge of the sensor time constant. After correction, lag errors are expected to be no larger than 1/5 of those shown, typically less than 0.1°.

When the sensors are first deployed or exposed, another kind of lag – the initial transient – is exhibited, since the sensor temperature at deployment can differ by several hundred degrees in the aeroshell phase from that to be sensed. Numerical simulations show, however, that within 1 to 3 seconds, the sensor temperature attains and crosses the recovery temperature curve, and thereafter follows it as described above. The initial transient period in the parachute phase is also of the order of 3 seconds to come within 3° of recovery temperature, from an initial temperature difference of 100°.

Conduction errors are driven by the temperature difference between the support posts and the thermocouples, and result from the slower response of the support posts. A representative case was analyzed in detail. The initial support post temperature in the aeroshell phase was assumed to be 425° below the flow recovery temperature. It required 18 seconds to cross the recovery temperature, and thereafter lagged the decreasing recovery temperature from above, by up to 40°. These temperature differences were used as end conditions to calculate the errors due to conduction $\delta T_c$ shown in Figure 9, from an exact equilibrium expression for conduction in long wires.

$$\delta T_c = (T_{sp} - T_r)[\cosh l/d \sqrt{Nu(k_s/k_w)}]^{-1}, \tag{11}$$

where $T_{sp}$ is support post temperature, $l/d$ is the wire length to diameter ratio, Nu is the Nusselt number of the wire, and $k_s/k_w$ is the ratio of gas to wire thermal conductivity evaluated at the stagnation temperature. The conduction errors are almost negligible for the aeroshell phase, because of the wire length and the good thermal coupling of the sensor wires with the atmosphere. They will, nevertheless, be corrected in the flight data.

In the parachute phase (in this example, below 7 km altitude), conduction errors are somewhat larger due to the higher thermal conductivity of the iron wire (which also makes the conduction asymmetrical) and they persist for a longer time because of the slow response ($\tau \sim 20$ sec) of the support posts in this phase. The support post response is illustrated by the following: If the posts are initially 70 °C warmer than recovery temperature, it takes about 50 seconds for them to attain and cross over the recovery temperature (at $z = 4$ km), after which they lag the recovery temperature by about 12° from below, at equilibrium. These temperature differences drive the conduction errors shown in Figure 9 for the parachute phase. The errors are subject to analytical correction post-flight, when the atmospheric properties and trajectory actually followed will be known. Residual errors after correction should be of the order of 0.1 those shown – that is, from 0.1° to 0.4°.

Radiation errors in the aeroshell phase are driven by the heat shield radiation, planetary surface radiation, and by sensor emission. Fortuitously, the heat shield temperature tends to be near the sensor temperature early in the use sequence when the lander velocity is still relatively high. For example, at sensor deployment, the atmospheric recovery temperature is nominally 700 K and the heat shield temperature has been bracketed by the contractor's estimates at between 520 and 580 K. Thereafter, the heat shield cools fairly rapidly (depending on atmospheric convection, and hence on the atmosphere and trajectory parameters). For example, it is estimated to cool to 400 °K in about 40 seconds. After the initial instant, in which sensor emission predominates, lander radiation absorbed by the sensor becomes the principal source of radiation error. Planetary radiation cannot be neglected, however, particularly if entry is at a time and site where the planet surface is warm (near 300 K). These considerations were used in a quantitative estimate to place limits on the radiative errors for the aeroshell phase, shown in Figure 9. Sensor wire emissivity

was allowed to differ from chromel and alumel and to vary with wire or source temperature, but it is a number near 0.2. The error range shown allows for various estimates of the heat shield surface temperature given by the contractor and for planet surface temperatures from 200 to 300 K. The uncorrected error magnitude is estimated not to exceed 2°, and to lie typically between 0.2° and 1.3°. When corrections are applied post-flight, it is expected that the residual errors due to radiation will be about $\frac{1}{4}$ this great, or typically 0.1° to 0.3°.

In the parachute phase, the deployed sensor on the lander footpad is exposed to thermal radiation from the lander just $\frac{1}{2}$ meter above, and to planetary surface radiation. The exact temperature relationship of the sensor, planet, and lander at the time of entry will not, of course, be established until the actual event, but some representative conditions have been analyzed. The three temperatures which govern the heat exchange – sensor, lander, and planet – are not far different. The view factor problems are complicated and not amenable to exact treatment. However, the worst case errors, shown in Figure 9, are expected to be less than 1°, and occur with the maximum lander temperature presently envisioned (336 K) and the planet surface at its maximum temperature of 300 K. These errors also are correctable post-flight, within the limits of uncertainties in emissivities, in lander component temperatures, view factors, and planet emissivity. The emissivity of the iron wire is high ($\sim 0.4$) and presents a special problem, because of its sensitivity to oxidation. For this reason, the lander sensor was protected within a desiccant cover when not required to be exposed, at all times from manufacture to launch. (Because of the corrosion susceptibility of iron, it is the author's opinion that a more chemically inert thermocouple material should have been used for this sensor.) However, the residual radiative error in this phase should not exceed the order of a few tenths of a degree.

The errors due to incorrect evaluation of the kinetic temperature contributions are very small for the parachute phase, as stated earlier. The kinetic temperature increments do not exceed 30°, initially on parachute deployment, and more representative value over the descent is 2° to 5°. Knowledge of the correction for this phase is estimated to be within about 1.2%. (Errors in recovery factor $r$ should be no larger than 1%, and errors in the velocity, redundantly defined by TDLR, radar altimeter, and descent phase measurements of $p$, $T$, and $a$, are expected to be less than 0.5%. Knowledge of the composition, and hence $c_p$, is expected to be comparably exact post-flight.) Hence, the kinetic temperature estimation errors are within the range of 0.02° to 0.36°, as shown for this phase in Figure 9.

In the aeroshell phase, the kinetic temperature uncertainty will be the dominant error source, especially in the early stages. The estimate shown assumes an uncertainty in the recovery factor $r$ of 1%, but it may be possible by means of ground facility calibrations still in progress to reduce this source of uncertainty by $\frac{1}{2}$. The other source of uncertainty evaluated is in the entry vehicle velocity, which, because of the excellence of the accelerometer data expected, is only 0.3% at sensor deployment when the kinetic contribution to the temperature is largest. As the velocity uncertainty grows (to 1.3% at the parachute deployment), the kinetic

temperature increment diminishes, so that velocity uncertainty never becomes a major error source. The uncertainty in gas composition has not been included in the estimates, but it is expected to be small, given data from two mass spectrometers.

A summary of the measurement error magnitudes after planned corrections are applied is given in the following table:

| | *Aeroshell phase* | *Parachute phase* |
|---|---|---|
| Response lag | 0.5° to 0.1° | 0.1° |
| Conduction | Negligible | 0.4° to 0.1° |
| Radiation | 0.3° to 0.1° | 0.25° |
| Root sum square | 0.6° to 0.14° | 0.5° to 0.3° |
| Kinetic temperature error | 5° to 0.8° (<2° below 24 km) | 0.36° to 0 |
| Probable error | 5° to 1° (<2° below 24 km) | 0.6° to 0.3° |

These errors must be combined with calibration errors (0.1° to 0.7°) and errors contributed by telemetry and electronics (about 1°) to obtain an overall expected accuracy figure of 1.7° to 2.5° in the aeroshell phase below 24 km, and 1.25° in the parachute phase. It is interesting that in the parachute phase, the largest single error source is the electronics.

### 3.4. Pressure sensors

The variation of stagnation pressure with altitude for a representative Viking entry into a model of the atmosphere of Mars is shown in Figure 10. During the high speed phase, the momentum of the atmosphere relative to the spacecraft multiplies the ambient pressure by a factor as large as 650 at the sensor inlet. As a result, pressure becomes measurable at relatively high altitudes by what can be termed continuum or conventional techniques, as opposed to low density techniques. For example, at 80 km altitude, ambient pressure in the model atmosphere employed here is 0.002 mb (1.5 $\mu$m Hg), but the stagnation pressure sensed on the entry vehicle is 1.3 mb. The latter figure is convertible to the former through well established relationships involving known parameters. If the measurement threshold is defined to occur at 4 resolution elements of the telemetry, i.e., at 0.6 mb, threshold will occur at an altitude of about 85 km in this model.

Stagnation pressure rises to a peak at an altitude near 34 km, due to the increase in ambient pressure, and thereafter decreases, due to the rapid decrease in vehicle velocity. Prior to the end of the aeroshell phase, the ratio of the measured to ambient pressure falls below 1.5. Then, after the parachute is deployed and velocities of descent decrease to the order of 50 m/sec, the presence sensed is essentially identical with ambient.

There are two science pressure instruments on each Viking entry vehicle, one on the aeroshell and one on the lander. They are different designs, produced by different manufacturers, although both sense the pressure from the deflection of thin,

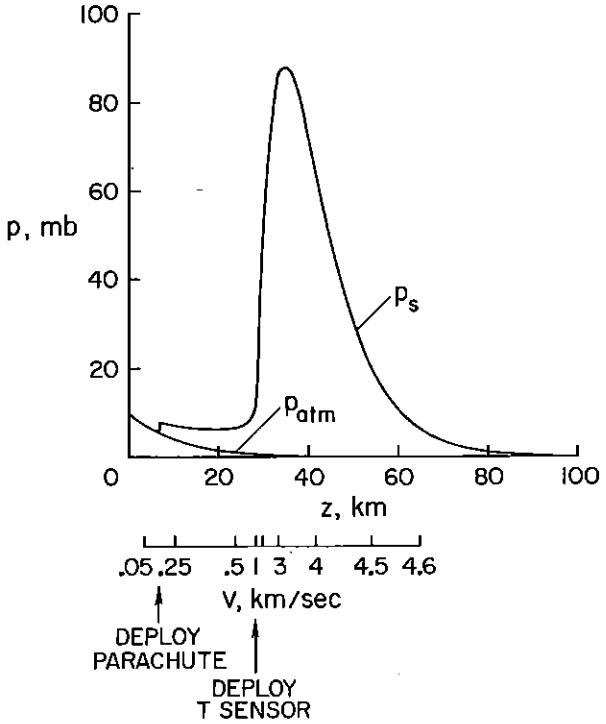


Fig. 10. Representative variation of stagnation pressure with altitude during Viking entry.

stretched stainless steel diaphragms, about 1 inch in diameter, which are referenced to sealed chambers at vacuum. The lander unit, which has a range of 0 to 18 mb and is used during parachute descent and in landed metereology, is basically the Tavis Model P4A, designed and manufactuered by the Tavis Corporation, Mariposa, California. The aeroshell unit has dual range outputs for 0 to 150 mb and 0 to 20 mb, and is used during high speed entry down to the point of aeroshell jettison. It was manufactured by K. West in Westminster, California, under the model designation 421-01. This latter sensor was a special purpose development for Viking, derived from a smaller sensor used on Skylab, and was produced under the technical direction of Richard McGunigle. Instrument engineers at Martin Marietta Aerospace were Frank Wiens, for the aeroshell sensor, and George Baker, for the parachute sensor.

A cross sectional drawing of the aeroshell sensor is shown in Figure 11, and photographs of the two sensors are shown in Figure 12. They are comparable in weight (~0.4 kg) and size (sensor cases are 10 and 7.6 cm long by 4 and 6 cm in cross section). The Tavis sensor shown in Figure 12(b) is a preliminary test model. Its case accommodates the sensor and the associated signal conditioning electronics. The valve attached to the pressure inlet is not a part of the flight hardware. The K. West aeroshell sensor case, Fig. 12(a), also accommodates its electronics and an internal

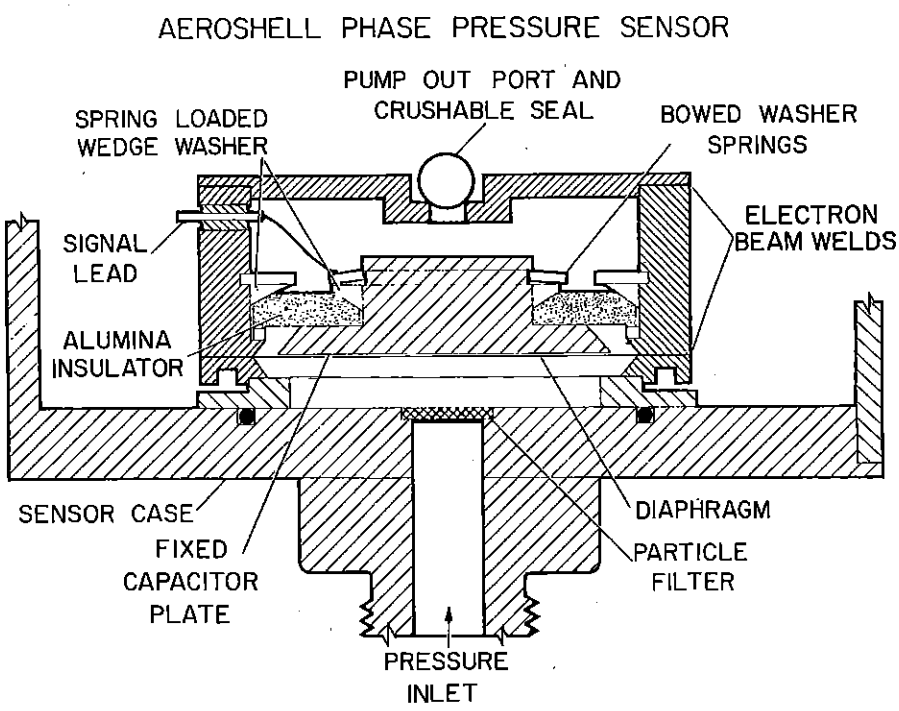


Fig. 11. Aeroshell pressure sensor schematic drawing.

temperature sensor, mounted on the back side of the sensor body. The black and metallic thermal control finish is evident. The internal temperature sensor will be used to correct for temperature effects on the calibration. The parachute phase sensor will also require temperature correction, but its temperature, by decision of the systems contractor, will have to be deduced from temperatures measured nearby on the lander structure.

The low pressures sensed by these instruments cause extremely small diaphragm deflections. For example, the aeroshell sensor diaphragm deflects nominally 0.02 mm at 150 mb pressure, so that a change of 1.5 mb (1% FS) corresponds to a deflection increment of only 0.2 $\mu$m. As a consequence, any rest state translation of the diaphragm relative to the sensing plate of 0.2 $\mu$m (8 microinches), due to thermal effects or mechanical relaxation, causes a 1% zero shift. The diaphragm tension is a parameter in this sensitivity. A relatively high tension was chosen and was thought to be optimum by the designers from an overall accuracy and repeatibility standpoint.

Diaphragm deflection is sensed by a capacitance pick up in the aeroshell sensor (Fig. 11), with the sensing plate on one side of the diaphragm; and by an inductive pick up in the parachute sensor, with coils on both sides of the diaphragm. The use of the symmetrical pick up appears to offer a stability advantage, in that translations of the diaphragm relative to the sensing elements tend to be symmetrical when

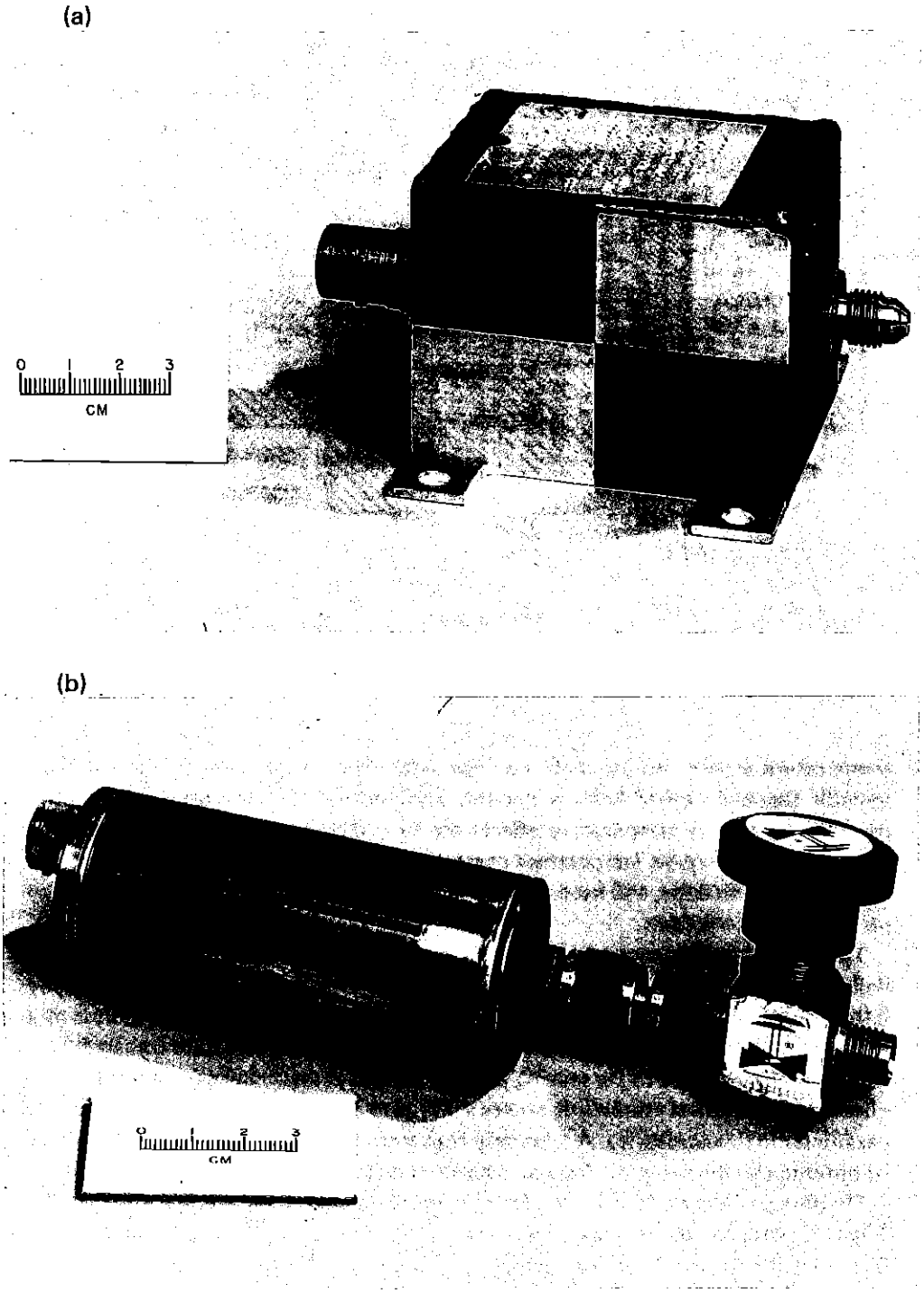


Fig. 12. Photographs of the pressure sensors: (a) Aeroshell phase sensor; (b) Parachute phase sensor.

temperature changes, e.g., and do not alter the zero reading. Scale factor varies with temperature however, and electronic temperature compensation is employed on the Tavis instrument. By decision of the author, it was elected to compensate for temperature shifts of the K. West instrument by use of multiple calibrations over a range of temperatures.

The primary measurement accuracy problems encountered in the test evaluation of these instruments have been, as suggested above, with zero-pressure signal stability, and with temperature sensitivity. Scale factor variations with temperature are at a moderate level and are relatively stable, at thermal equilibrium, although some thermal hysteresis is evident, particularly on the aeroshell instrument, and there are effects of temperature rate as well as temperature. The data will be summarized below.

For Entry Science purposes, the zero stability is required only for a very short time period, since the instrument signal at zero pressure is read immediately prior to entry and the entire measurement sequence is then completed in a period of approximately 5 minutes. Within this period, the sensors experience vibration, shock, and temperature rise. The scale factor must be stable over a period of months, however, from the last prelaunch calibration. For the landed meterology investigation, long term total stability is required of the lander instrument, over a time period of three months. This aspect of the instrument's use has been investigated by the Viking Meteorology Team.

Electrically, the sensors require about 1 watt (aeroshell sensor) and 0.16 watt (lander sensor) at 28 volts DC, and delivery nominally 0 to 5 volt analog signals. (The aeroshell sensor span on low range is more nearly 2.5 v.) The sensors were designed to operate accurately over a range of 24 to 37 volts input, and in the presence of some fairly severe voltage transients and noise and ripple on the power line.

Telemetry resolution is eight bits, so that pressure resolution in the aeroshell phase is nominally 0.6 mb on 150 mb range, and better than 0.16 mb on 20 mb range. In the parachute and landed phases, it is nominally 0.07 mb. Sampling rates are two per second prior to reaching a deceleration of 0.05 g, five per second during the remainder of the entry phase to aeroshell jettison, and two per second again during parachute descent. Altitude resolution over the entire entry period, altitudes from 100 to 7 km, is always better than 500 m, to a minimum of 7 m at 38 km altitude. In parachute descent, altitude resolution is of the order of 30 m. The parachute phase instrument is read at 1 sps during the entry phase, while exposed only to capsule internal pressure, in order to permit its stability of response through the entry vibration and thermal environments to be evaluated.

The sterilization requirement, much feared in advance for all Viking instruments, caused fewer problems than expected. The Tavis instrument is normally artificially aged at temperatures higher than sterilization to improve its stability, so it has caused no problems. Neither did the design of the K. West instrument suffer any major restrictions due to sterilization. A remaining impact of sterilization, however, is its effect on the instrument calibrations. The scale factor must be stable through final

sterilization, since no calibrations can be performed thereafter. This characteristic was evaluated in tests incorporating simulated sterilizations.

Another concern felt in advance which caused little trouble was the problem of maintaining high vacuum in the small volume reference chambers of the sensors, over the long period from manufacture to use. None of the instruments accepted for test or flight applications have shown evidence of leakage. Zero shifts are seen, but are random in nature, and not progressive as they would be if due to leakage. The K. West sensor body is electron beam welded, and the reference volume is evacuated through a hole in the sensor base, which is then sealed by crushing a hardened stainless steel ball into the sharp corners of the hole edge.

The test program disclosed a few failures of subelements of the sensors in the shock and thermal tests, due to connections being broken by differential expansion and insulators by shock, etc. It was possible to find corrections for these problems in every case. We will not review them here in detail.

*Calibration.* The sensors were calibrated against fused quartz pressure gages (Texas Instruments model 141) accurate to within 0.015% of reading, which were calibrated against laboratory standards within the preceding three months. Calibrations were performed on some sensors in more than one laboratory (e.g., at K. West or Tavis, Martin Marietta Aerospace, and Ames Research Center), with basically similar equipment. Three different gases were used in calibrations at Ames, and, as expected, no differences in response were detected.

A representative room temperature calibration is shown for the dual range aeroshell sensor in Figure 13(a), and for the parachute sensor, in Figure 13(b). Both sensors are characteristically near linear in output. Hysteresis is usually less than 5 mv, or 0.1% of full scale, for pressure increasing and decreasing. This is also the order of the short term total scatter in readings at constant environmental conditions.

*Environmental Effects on Stability.* The effect of temperature on the calibration of a typical parachute phase sensor is shown in Figure 14. Two sets of data are shown, one obtained at Tavis Corporation (square symbols) and the other at Martin Marietta Aerospace (circles). The data were collected in April and May of 1974 as part of the Acceptance Test Program. A multiple sterilization thermal cycle (called a heat compatibility test), and a test vibration sequence (both sinusoidal and 6g rms random) were included in this test sequence, and their effects on the calibrations can be evaluated.

The zero pressure signal, shown in the lowest graph of Figure 14, varies in each set of data by about 0.1 mb over the 180°F temperature range. The temperature dependence is comparable in the two sets of data. The incremental signal due to applied pressure, $S-S_0=\Delta S$, given in the upper four plots for pressures of 3.6 to 17.9 mb, shows very small scatter about the faired curve drawn through each set of data, of the order of a few hundredths of a millibar. There are systematic differences between the two sets of data which indicate a scale factor shift (1%) and a zero shift

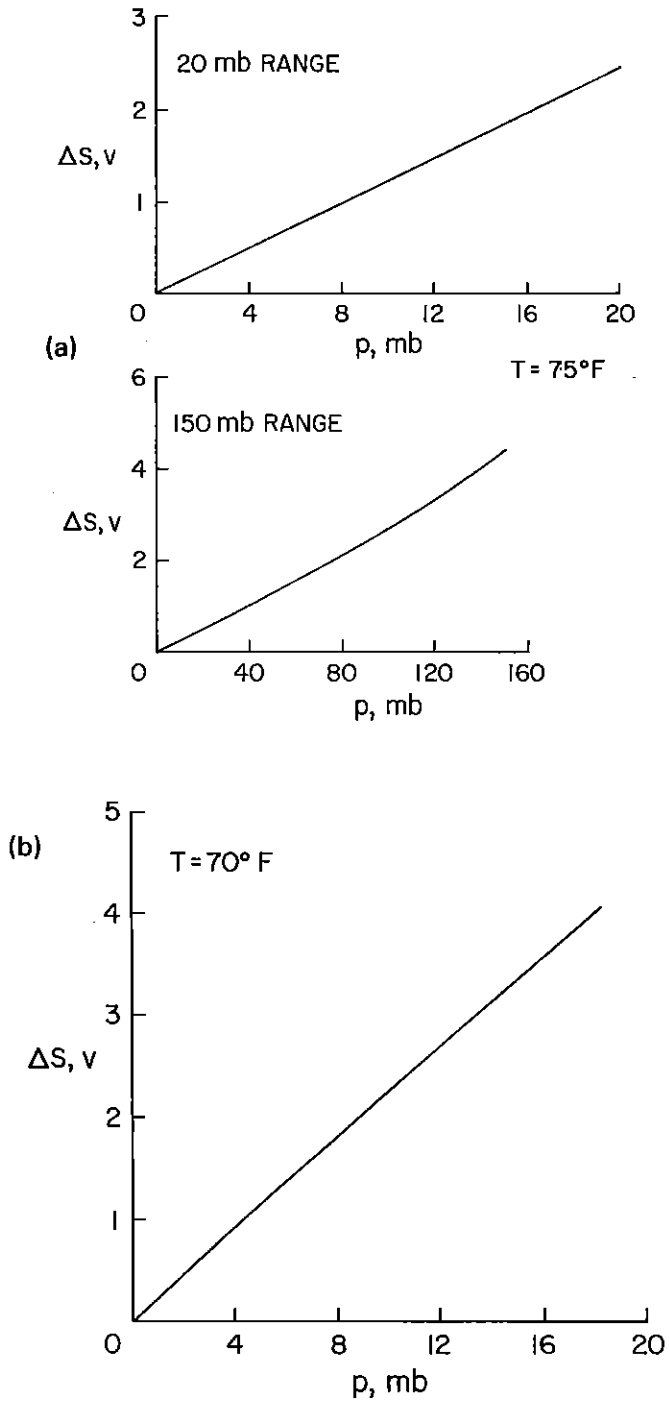


Fig. 13. Pressure sensor calibrations: (a) Aeroshell phase; (b) Parachute phase.

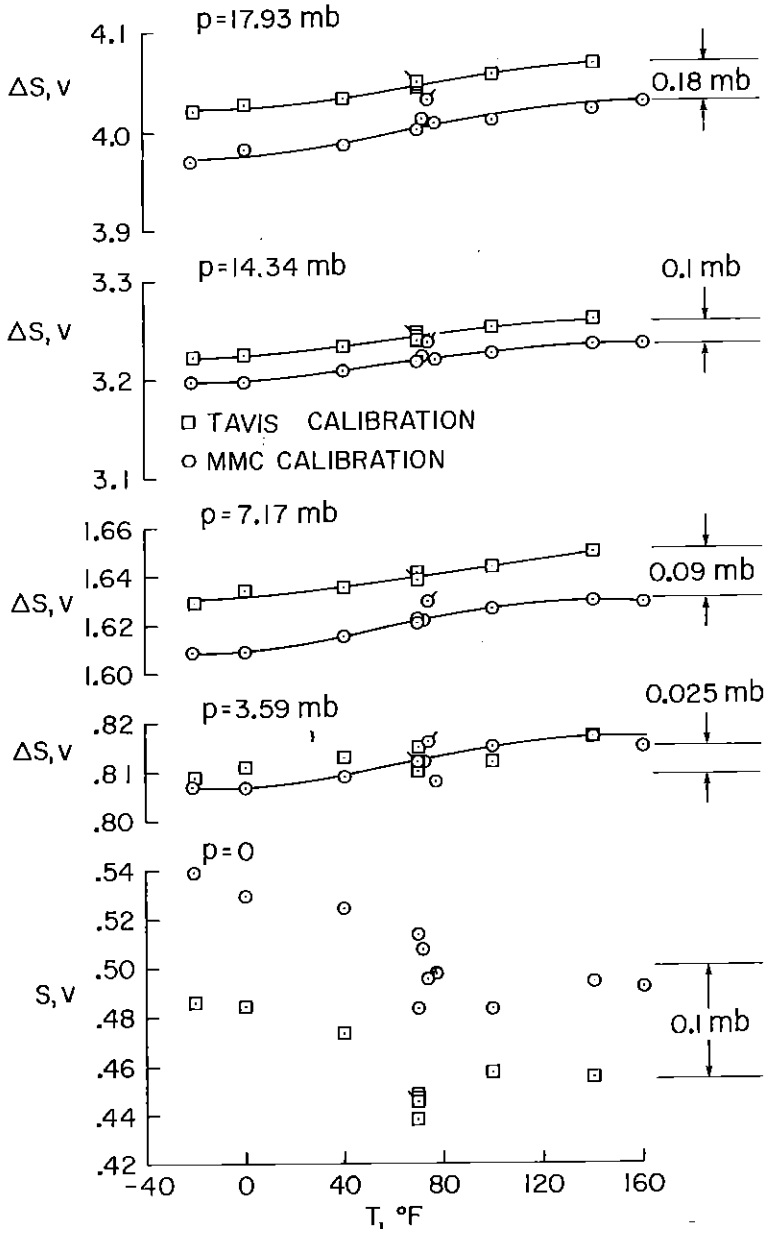


Fig. 14. Temperature sensitivity of the parachute phase pressure sensor.

(0.1 mb). The scale factor differences were partly a result of limited accuracy of the calibration standard used at Tavis, which was another Tavis sensor which had been calibrated against a water manometer.

The effects of the test environments can be identified from the data. The flagged square symbols in the figure show data at Tavis before the multiple sterilization test. All other points were taken afterwards. The flagged circles represent pre-vibration

test points at Martin Marietta. It is evident that the sterilization cycles at Tavis (233 °F for 54 hours) did not significantly affect either the zero reading or the scale factor. Vibration apparently did affect the scale factor, however. Notice the flagged circles, the pre-vibration points, in the upper four plots, the first data taken at Martin Marietta immediately following the Tavis test program. They tend to agree with the Tavis data at the four non zero pressure levels. The effects of the vibration test are further displayed in Figure 15, the variation with time of room temperature

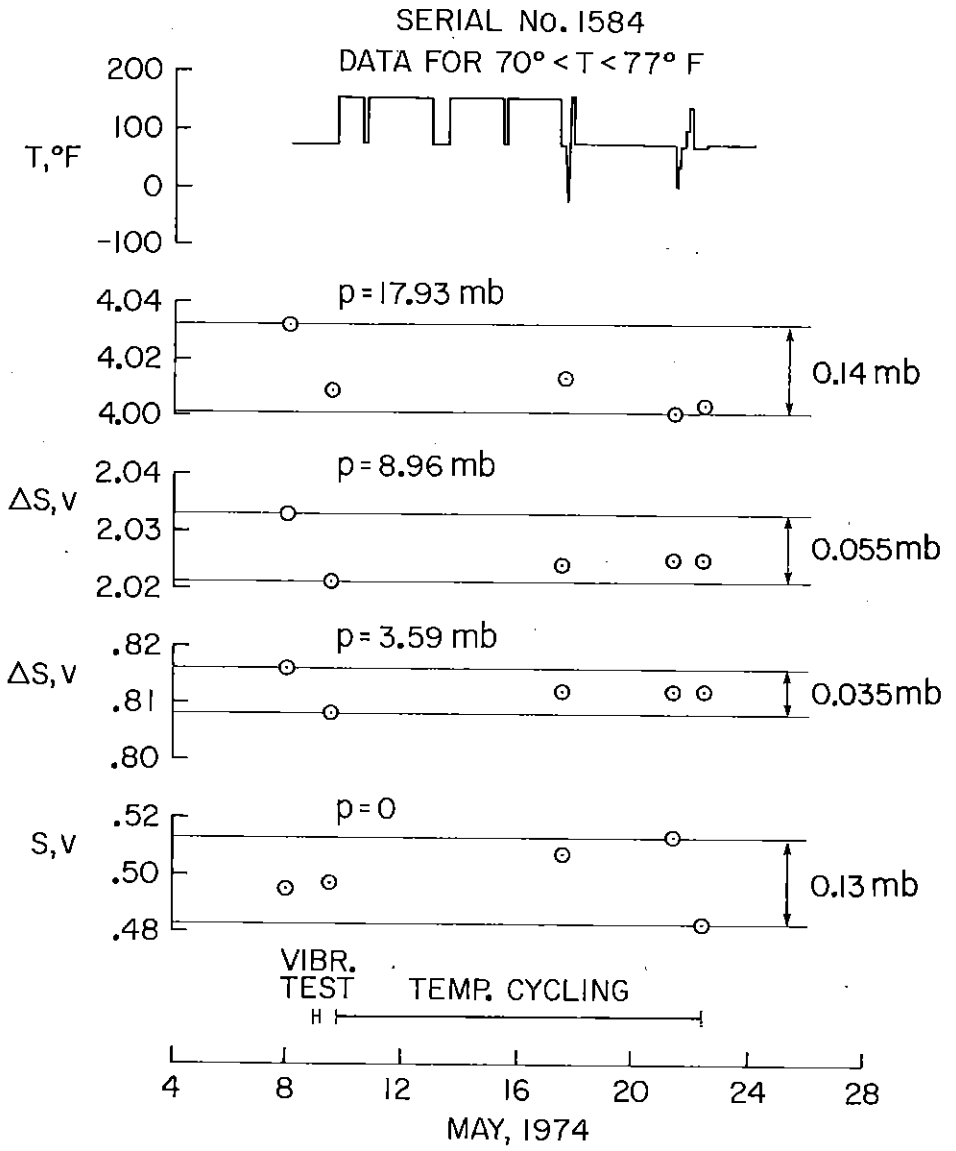


Fig. 15. Zero reading and scale factor stability through the acceptance test program, parachute phase pressure sensor.

calibration data through the test sequence at Martin Marietta. The instrument scale factor was decreased by the vibration test performed on May 9 by as much as 1%. Thereafter, it held constant, to within hundreds of a millibar, through temperature cycles rather extreme compared to those expected in flight. Zero readings were affected by these temperature cycles, however, by as much as 0.13 mb.

To summarize: The calibrations were not affected by sterilization. Scale factor shifts of about 1% (0.06 mb at 6 mb) were seen after vibration. Zero readings were unaffected by vibration, but there was a 0.1 mb zero shift between the Tavis calibration program and the Martin program. The cause of this shift is not evident, but it could have been due to handling shock and vibration in transit from California to Colorado.

The zero reading of this sensor, which will be taken just prior to entry into the atmosphere of Mars, could change prior to the parachute descent by as much as 0.02 mb due to entry vibration and perhaps as much as 0.05 mb due to entry thermal changes (less than 20 °F in 20 minutes), on the basis of the above data. Changes of the order of 1% in scale factor, due to vibration, also could occur subsequent to the final calibration. If the zero shifts occur prior to parachute descent, they should be seen in the data sent during this period. It is thus expected that the measurements in parachute descent will be significant to within about 0.05 mb (40 $\mu$m Hg), or to the order of 1% of reading.

Similar test data for one of the flight aeroshell sensors are shown in Figures 16 through 18. In Figure 16, temperature sensitivity of the scale factor is plotted as incremental voltage above the zero pressure signal. The data were collected over a 32 day period in the acceptance test program, and include effects of environmental testing – heat compatibility, thermal cycling, and vibration. Data for temperature rising have been separated, for correlation purposes, from those for temperature falling, and are compared with the latter for pressures of 10 mb and 60 mb. The temperature sensitivity of the scale factor is small, and repeatibility is typically within $\pm 10$ mv scatter about the mean on low range ($\pm 0.08$ mb), and less than $\pm 6$ mv or $\pm 0.2$ mb on high range.

The zero pressure signals, shown in Figure 17, are considerably less stable. As discussed earlier, these zero shifts correspond to very small changes in the diaphragm-to-sensing-plate spacing, and it has not been possible to associate them with a particular cause. They are stimulated by temperature cycling the sensor, especially at large temperature rates, but also change with time without the sensor being handled or used.

At room temperature, a range of zero readings with a pressure equivalent of over 1 mb was recorded. However, the question to be addressed is change in zero reading to be expected in the 10 minutes from just prior to entry to the end of the aeroshell phase of the entry. Data shown in Figure 18 bear on this question. They were taken at room temperature, with temperature rising (the expected direction of change during entry), and are plotted against the date on which they were taken, and related to the sequence of tests in the acceptance program.

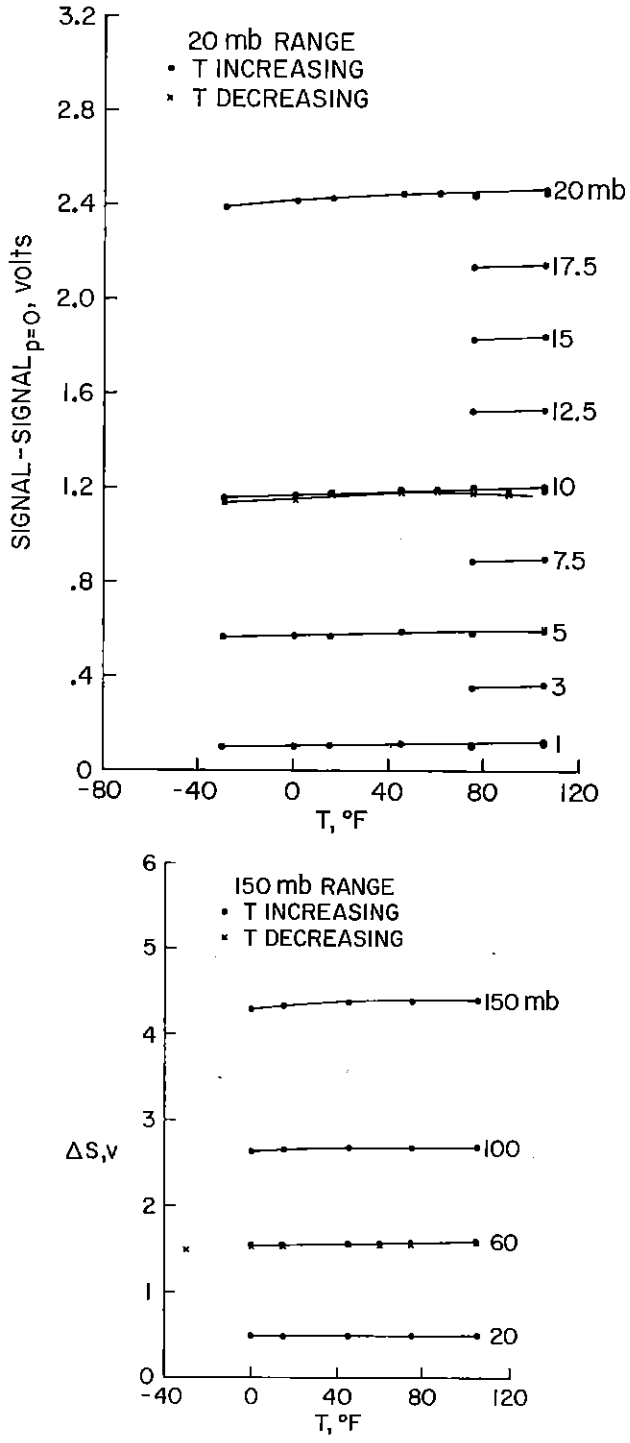


Fig. 16. Temperature sensitivity of the scale factor of the aeroshell pressure sensor.

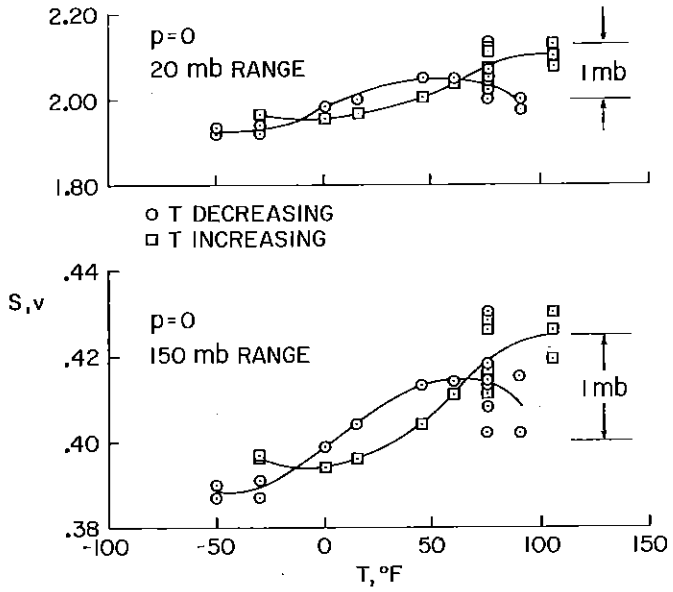


Fig. 17. Zero reading stability of the aeroshell pressure sensor.

The largest zero shifts were excited by the thermal vacuum tests, March 1 to 4, in which temperature was cycled from −15° to 105 °F six times in typical heating and cooling times of 30 minutes and 20 minutes. However, the entry thermal cycle, simulated in the test on March 5 by a 20 °F temperature increase in 10 minutes, caused zero shifts of from 0.08 to 0.16 mb. The 10.6 g rms random vibration test, applied in all three axes on February 27, plus the sinusoidal vibration test the same day, gave rise to a shift of 0.05 to 0.10 mb. This order of stability against the short term entry environments has been indicated both by the flight sensors and the qualification test sensor at higher values of the test parameters, and gives assurance that unknown zero shifts during entry should not exceed 0.2 mb. Zero shift errors in the ambient atmospheric pressure derived from measured stagnation pressure are, of course, smaller than this value by a factor which is the ratio of ambient to stagnation pressure (see Figure 10).

The stability of the scale factor through sterilization is indicated by the comparison of readings on February 8 and 19. At pressures of 5, 10, 60, and 100 mb, changes ranged from 0.02 mb to 0.33 mb. The overall spread of scale factors through the acceptance tests gave rise to scatter of the signals of nominally ±0.4% of reading at the higher three pressures, and ±1.8% of reading at 5 mb. Hence, it is expected that the aeroshell sensor will define the pressures applied to it by Mars atmosphere to within 0.2 mb (zero shift) ±0.4% of reading (scale factor) at and above 10 mb stagnation pressure; and within 0.2 mb ±1.8% of reading at 5 mb. The probable errors are smaller than these linearly combined estimates of maximum error seen in the tests.

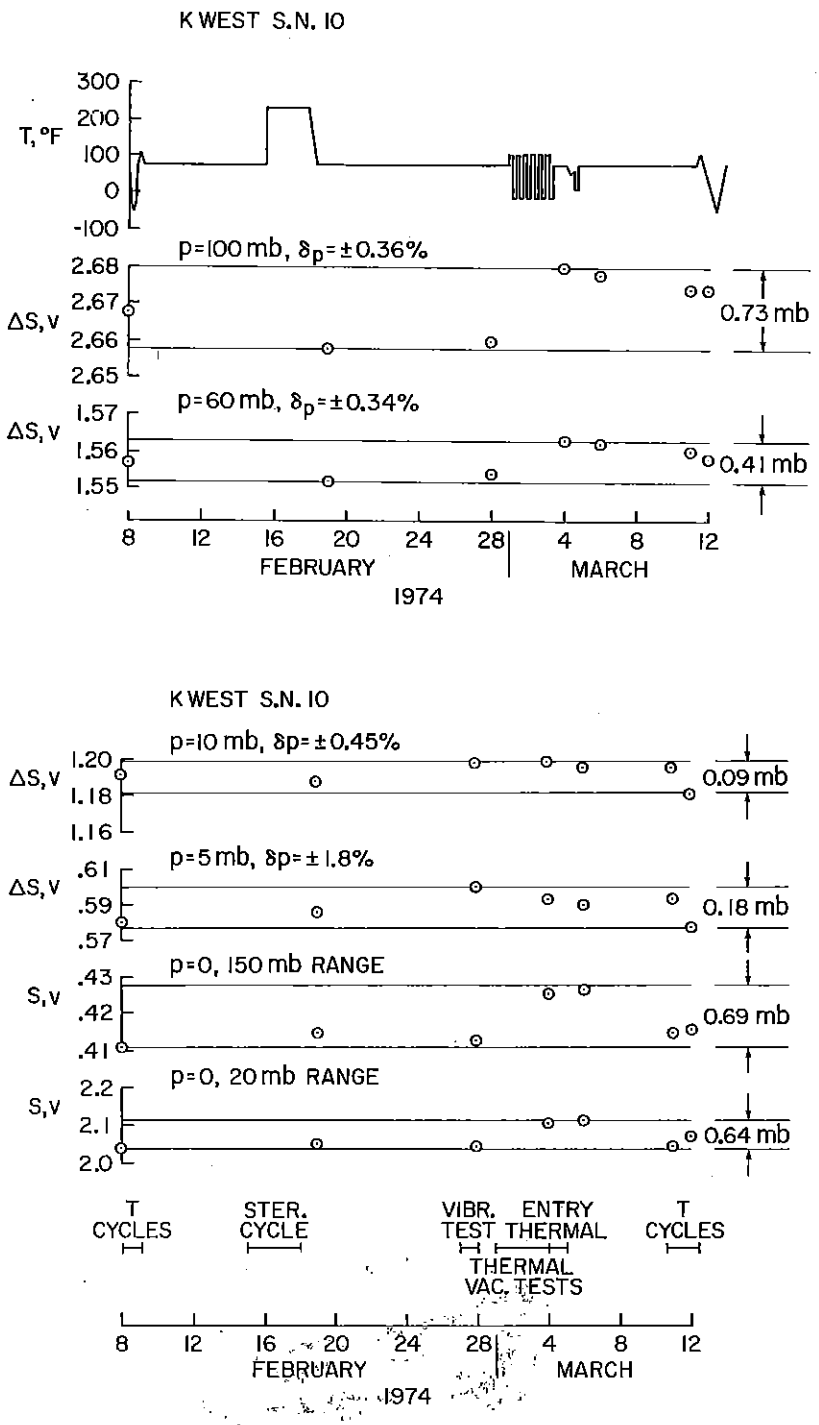


Fig. 18. Zero reading and scale factor stability through the acceptance test program, aeroshell phase pressure sensor.

*Measurement Errors.* A listing of possible measurement errors due to factors other than the sensors includes for the pressure measurement: (1) Errors due to port location, port geometry, or vehicle attitude. (2) Error in knowledge of the ratio of the measured stagnation pressure to ambient pressure. (3) Response lag in the sensor inlet tubing. (4) Leaks in the sensor inlet plumbing. A few remarks on each of these is given below, followed by a summary of expected errors in pressure measurement in the Mars atmosphere.

The aeroshell sensor port has been located to be on the stagnation point of the entry vehicle at its trim angle of attack. If angle of attack differs from that expected (by perhaps a few tenths of a degree), the inlet pressure changes will be negligible. At 2° change in angle of attack, the change in inlet pressure is less than 0.1%. Hence, this is not a significant error source.

Similarly, the parachute pressure inlet was designed as a Kiel probe to reduce the sensitivity of the measurement to the direction of the local streamlines. Tests and calculations have shown that the inlet pressure will be within 0.1% of stagnation pressure for vehicle angles of attack to 21°, or combinations of angle of attack and deviations of actual flow direction from the expected flow direction totalling 21°.

Since stagnation pressure is measured and ambient pressure is desired, the following relationship is invoked to make the conversion,

$$p_s/p_\infty = C_{p_s}\mu V^2/2R_u T_\infty + 1 \tag{12}$$

(compare with Eq. (9)). Errors are introduced by inexact knowledge of $C_{p_s}$, $\mu$, $V$, and $T_\infty$. Here, $C_{p_s}$, the stagnation pressure coefficient, ranges from 1 in incompressible flow to an upper limit of 2 in hypervelocity flow, and is known theoretically, given the gas composition. For conditions representative of the parachute descent, the pressures $p_s$ and $p_\infty$ will differ by about 6.5% of $p_\infty$. The ratio $p_s/p_\infty$ will be known within about 0.75% post-flight, so the resulting error in $p_\infty$ is $0.0075 \times 0.065$ or 0.0005, or 0.05%.

At the time of temperature sensor deployment in the aeroshell phase, defined as the beginning of the low speed phase of the experiment, the ratio of stagnation to ambient pressure is much greater, about 35. Then, for expected uncertainties in $V$, $T_\infty$, $C_{p_s}$, and $\mu$, the uncertainty in $p_s/p_\infty$ is approximately 0.7%.

During the very high speed phase, when the ratio of measured to ambient pressure will rise to the order of 650, accuracy of knowledge of the ratio is expected to be within about 3 percent. This uncertainty reflects directly into the deduced ambient pressure.

Response lags in the inlet tubing have been restricted by selection of tubing length and diameter to less than 0.1 second for both the aeroshell and parachute phases. The largest response lag pressure error in the terminal descent, after the lander is slowed to equilibrium descent velocity, occurs at the lowest altitude, and is governed by

$$\delta_{p_t} = -\tau \rho V g. \tag{13}$$

The maximum magnitude of $\delta_{p_t}$ is 0.003 mb, well within the sensor accuracy and the telemetry resolution limits. At parachute opening, the magnitude of the pressure error due to tubing response is 0.01 mb.

In the higher speed phases, the lag error is less than 2 percent for stagnation pressures above 1 mb, and below 1 percent for pressures above 10 mb. In the analysis of a typical entry, the lag error remained below 0.5 percent from an altitude of 40 km to the end of the aeroshell phase.

The tubing connections and sensors were checked after installation in the spacecraft by means of pressure stimuli applied by a vacuum test system incorporating as a comparison standard an accurate bourdon tube vacuum gage. Agreement with the standard gage was within the resolution error, 0.16 mb. Sensor readings were taken through the spacecraft data system. No detectable errors due to leaks were disclosed in this test sequence, either by reading comparisons with the standard gage, or by some simple rate-of-rise tests.

*Summary of Error Estimates.* The table below summarizes errors expected in direct sensing of the atmospheric pressure at Mars in three different phases of the entry, from all recognized sources. It lists the altitude range and the pressure range in each of three phases. Pressure range is given in terms of measured stagnation pressure, and also as ambient atmospheric pressure. Errors listed include those due to the sensors, sensor installation, and telemetry. The root-sum-square error in measured (stagnation) pressure is combined with the conversion error from stagnation to ambient pressure, expressed in the table as an equivalent error in stagnation pressure. Finally, errors expected in ambient pressure are given, both in millibars and

| | Parachute descent | Aeroshell, $V<1$ km/sec | Aeroshell, High speed |
|---|---|---|---|
| Altitude, km | <7 | 7 to 25 | 25 to 80 |
| Measured pressure range, mb | 3 to 10 | 6 to 16 | 1 to 100 |
| Ambient pressure range, mb | 3 to 10 | 4 to 0.5 | 0.0016 to 0.5 |
| Sensor errors | | | |
| Undetected zero shifts, mb | 0.05 | 0.2 | 0.1 |
| Scale factor, mb | 0.05 | 0.08 | 0.004 to 0.4 |
| Measurement errors, mb | | | |
| Port orientation | <0.005 | <0.01 | <0.1 |
| Response lag | <0.01 | <0.02 | 0.02 to 0.2 |
| Telemetry, single rdg., mb | 0.07 | 0.16 | 0.16 to 0.6 |
| Root-sum-square error in measured pressure, mb | 0.08 | 0.23 | 0.12 to 0.5 |
| Conversion errors, $p_s$ to $p_\infty$, expressed as error in $p_s$, mb | 0.005 | 0.1 | 0.03 to 3. |
| Resultant error in ambient pressure, mb | 0.08 | 0.17 to 0 008 | 0.0002 to 0.01 |
| Percent | 2.7% to 0.8% | 4.2% to 1.6% | 12.5% to 3.6% |

percent. Where a range of values is given within one mission phase, the left and right hand entries are related vertically in the table, left with left, and right with right, throughout. Since the telemetry error of a single reading is reduced by data smoothing, 0.4 of the listed value has been included in forming the RSS values.

Notice that in the last column, the altitude limits do not correspond to the pressure limits (see Figure 10). Peak pressure occurs near 35 km, while the minimum pressure occurs at the threshold altitude. At 25 km, values from the middle column apply (1.6% resultant error). The 100 mb condition, for which estimated error is 3.6%, represents the peak in the $p_s(z)$ curve. The 12.5% error at measurement threshold is dominated by the 0.1 mb zero shift error, assumed constant through this phase. The threshold error is therefore somewhat arbitrary, depending on the definition of threshold. For example, if theshold is defined to occur at $p_s = 2$ mb, 75 km altitude, the initial error is 7%; if at 4 mb, 68 km altitude, initial error is 4.7%; etc. Except near the threshold, the overall expected errors in ambient pressure range from 1 to 4 percent over the entire altitude range of measurement.

### 3.5. Radars

No attempt will be made here to discuss the detailed design and technical characteristics of the two on-board radars which will provide data used by the Viking atmosphere structure experiment. We will, however, briefly describe them and list some of the expected performance characteristics. These instruments were produced under contract to Martin Marietta Aerospace by Teledyne Ryan Aeronautical in San Diego, and their development was managed by John C. Heising, who kindly has provided the information given below.

*Altimeter.* The radar altimeter uses time of first return of radio energy pulses reflected from the nearest planet surface to measure altitude over a range from about 135 km to 30 m. The altimeter is a high accuracy, short pulse system, with four separate modes, pulse widths from 0.05 to 6 $\mu$sec, and four repetition rates, to cover the broad range of altitudes. The 6 $\mu$sec pulse width is used throughout the aeroshell phase. Transmitted frequency is $10^9$ Hz (30 cm wavelength), at a peak pulse output power of 140 watts.

There are two complete, redundant altimeters on each lander. Only one is used at a time. Both are connected to the two antennas indicated in Figure 3, one on the forward face of the aeroshell, and one on the bottom of the lander. Each altimeter is packaged in a box $15 \times 20 \times 25$ cm, and weighs under 5.5 kg. Steady input power is 31 watts.

Martin Marietta Aerospace has made a detailed accuracy analysis of expected altimeter performance. Expected errors (3 sigma) range from 400 m at 70 km altitude and 135 m at 15 km altitude to 100 m at parachute deployment. On the parachute, a representative error is 35 m. "Residual terrain bias" is a primary error source.

*Terminal Descent and Landing Radar.* This system is a Doppler radar designed to measure the three components of lander velocity, at 5 samples per second, during parachute descent. It has four sensing beams, but functions with any three. The beams are 3.5° wide, and are independently powered, with four separate transmitters, to avoid single point failure. Operating frequency is $13.3 \times 10^9$ Hz (2.25 cm wave-length), with channel separation of $10^7$ Hz. The antennas are phased arrays, four in all, each about 0.3 m square, mounted in a flat panel about 0.75 m square. Two antennas transmit the radar beams, and two receive reflected energy from the planet surface. The antenna panel is the lower face of a thin box (8 cm thick) which contains the system electronics. Total weight is 22 kg, and power consumption is 97 watts. The directions of the four beams lie in planes perpendicular to the edges of the antenna panel, and are directed downward at an angle of 21° to the lander axis.

The Martin Marietta estimate of system velocity accuracy is, in the direction along the lander axis (approximately vertical), from 0.5 to 1.0% of descent speed; in the two directions perpendicular to the axis (approximately horizontal), from 1 to 3% of total velocity. Thus, for the lander axis vertical and in the absence of horizontal motion (in wind), at a descent velocity of 50 m/s, an uncertainty in horizontal velocity of 0.5 to 1.5 m/s would apply. For 50 m/s descent speed and 50 m/s horizontal velocity, uncertainty in the horizontal velocity would rise to 0.7 to 2.1 m/s. To convert the horizontal velocity to a wind measurement, the response of the lander on its parachute to the wind must be analyzed, and effects of rotational dynamics removed. Hence, the above uncertainty figures do not directly represent wind uncertainties, but they are expected to be of the order of the uncertainty in the deduced horizontal wind velocities.

## 4. Summary and Conclusions

Three groups of instruments will be used to define the structure of Mars atmosphere in situ, from roughly 100 km altitude to touchdown, when the two Viking landers enter the planet's atmosphere in 1976. These are inertial sensors (primarily accelerometers), pressure and temperature sensors, and radar altimeters and velocimeters. All have been briefly described herein, and their accuracies and error sources have been discussed.

The accelerometers alone will define the atmosphere structure from 100 km to about 20 km altitude, with supplementary altitude data from the altimeter. Below 20 km, direct sensing of pressure and temperature will be primary. During parachute descent, the vertical and horizontal wind velocities will be inferred from data taken by the lander Doppler radar. At higher altitudes, wind information will be derived from analysis of the vehicle attitude history transmitted by the gyroscopes. The terrain elevation profile beneath the landing track will be obtained from combined use of the radar altimeter and accelerometer records. The planetary radius at the landing site, needed for interpretation of the pressure data, should be defined to within a few tenths of a kilometer by the accelerometers.

The guidance accelerometers to be used for these purposes have been evaluated in test programs and are accurate to within 0.05%, at worst. This corresponds to a definition of local atmospheric density within 1% down to 20 km altitude, unless extreme winds are encountered, and the errors are actually predominated by other factors (uncertainties in entry velocity, vehicle drag coefficient, and mass). The corresponding errors in temperature for this high altitude region are expected to be the order of a few degrees Kelvin.

The temperature sensors used in the lower atmosphere should yield the ambient temperatures within about 0.5° below 8 km and within 2° below 24 km. The design (fine wire thermocouples, exposed directly to the atmosphere outside the vehicle boundary layer) was governed by the minimization of errors for the measurement conditions presented by the descent through the low densities of the Mars atmosphere, and the largest remaining error source appears to be possible drift in the resistance values in the electronics. It appears that telemetry resolution may limit the resulting knowledge of atmospheric temperature more so than instrument accuracy.

The pressure sensors are expected to give the atmospheric pressure within 1% to 3% in the lowest 8 km, and within 4% up to an altitude of 65 km. The key sensor design problem was stability of zero reading to the level of tenths or hundredths of a millibar, in the presence of preflight and flight environments. On the basis of a thorough test and evaluation program, it appears that sensor calibration stability to within 0.1 mb will be realized or closely approached. Over most of the altitude range, telemetry resolution again sets the limit on precision of a single reading.

The radars are capable of 35 to 400 m altitude accuracy, at altitudes from 100 m to 135 km; and of better than 2 m/s velocity accuracy after parachute deployment at 6 to 8 km altitude.

In combination, barring any unforeseen failures or catastrophic events, these sensors should provide a major improvement and extension of our accurate descriptive knowledge of the atmosphere of Mars, and hopefully, our understanding of its physics.

## References

1. Nier, A. O., Hanson, W. B., McElroy, M. B., Seiff, A., and Spencer, N. W.: 'Entry Science Experiments for Viking 1975', *Icarus*, **16**, no. 1, p. 74 (1972).
2. Seiff, A., Reese, D. E., Sommer, S. C., Kirk, D. B., Whiting, E. E., and Niemann, H. B.: 'PAET, An Entry Probe Experiment in the Earth's Atmosphere', Icarus, **18**, no. 4, p. 525 (1973).
3. Seiff, A. and Reese, D. E.: 'Defining Mars' Atmosphere – A goal for the Early Missions', *Astron. and Aeron.*, **3**, no. 2, p. 16. (1965)
4. Seiff, A. and Reese, D. E.: 'Use of Entry Vehicle Responses to Define the Properties of Mars Atmosphere', *Advances in the Astronautical Sciences*, Vol. 19, Amer. Astron. Soc., Washington, D.C., 1965, p. 419.
5. Seiff, A.: 'Direct Measurements of Planetary Atmospheres by Entry Probes', *Advances in the Astronautical Sciences*, Vol. 25, Amer. Astron. Soc., Washington, D.C., 1968.
6. Seiff, A.: 'Measurements in the Atmosphere of Mars', *Appl. Opt.*, **8**, no. 7, p. 1305 (1969).

7. Sommer, S. C., Boissevain, A. G., Yee, L., and Hedlund, R. C.: 'The Structure of an Atmosphere from On-Board Measurements of Pressure, Temperature, and Acceleration', NASA TN D-3933, Ames Research Center, Moffett Field, Calif. (1967).
8. Sammonds, R. I. and Kruse, R. L.: 'Aerodynamic Characteristics of the Planetary Atmosphere Experiments Test Entry Probe', *J. of Sp. and Rockets*, **12**, no. 1, p. 22 (1975).
9. Anderson, J. D., Efron, L., and Wong, S. K.: 'Celestial Mechanics', *Mariner-Mars* 1969, *A Preliminary Report*, National Aeronautics and Space Admin., Washington, D.C. NASA SP-225, p. 127, 1969.
10. Sjogren, W. L., Lorell, J., Wong, L. and Downs, W.: 'Mars Gravity Field Based on a Short-Arc Technique', *JGR*, **80**, no. 20, p. 2899 (1975).
11. Phillips, R. J. and Saunders, R. S.: 'The Isostatic State of Martian Topography', *JGR* **80**, no. 20, p. 2893 (1975).
12. Anderson, D. M., Biemann, K., Orgel, L. E., Oro, J., Owen, T., Shulman, G. P., Toulmin, P. III, and Urey, H. C.: 'Mass Spectrometric Analysis of Organic Compounds, Water and Volatile Constituents in the Atmosphere and Surface of Mars', *Icarus*, **16**, no. 1, p. 111 (1972).
13. Millard, J. P., Green, M. J., and Sommer, S. C.: 'Analytical Design of Sensors for Measuring Atmosphere Temperature During Planetary Entry', NASA TN D-6947, Ames Research Center, Moffett Field, Calif. (1972).
14. Dewey, C. F.: 'Correlation of Convective Heat Transfer and Recovery Temperature Data for Cylinders in Compressible Flow', *Int. J. Heat Mass Transfer*, **8**, p. 245 (1965).